Biogeosciences
Discussions

1

2

3

4

Modeling transient soil moisture limitations on microbial carbon respiration

7

8

9

10

11

12

13

14

15

Yuchen Liu[1*]; Matthew J. Winnick[2]; Hsiao-Tieh Hsu[2,3]; Corey R. Lawrence[4]; Kate Maher[2,5];
Jennifer L. Druhan[1]

1. Department of Geology, University of Illinois Urbana Champaign, Champaign IL 61820-6371, USA
2. Department of Geological Sciences, Stanford University, Stanford CA 94305-2115, USA
3. Department of Chemistry, Stanford University, Stanford, CA
4. United States Geological Survey, Denver
5. Rocky Mountain Biological Laboratory, PO Box 519, Crested Butte, CO 81224
*. Email: liu305@illinois.edu

26

27   **Abstract:** Observations show that soil microorganisms can survive periods of aridity and recover
28   rapidly after wetting events. This behavior can be explained by a moisture-dependent adaptation
29   (*i.e.* the ability to transition between a dormant state in dry conditions and an active state in wet
30   conditions). Though this dynamic behavior has been previously incorporated into modeling
31   frameworks, a direct comparison between a model application of this active-dormant transition
32   mechanism and a more simplified first-order model has yet to be made. Here, we developed two
33   models, one using simplified first-order kinetics and the other featuring a process-based rate
34   expression incorporating the transition between active and dormant biomass. The two approaches
35   are contrasted through a benchmarking exercise using a set of time series soil incubation datasets.
36   We evaluated the two models using an Akaike Information Criterion (AIC). Combining the AIC
37   evaluation and model-data comparison, we conclude that the dormancy-incorporated model
38   performs better for shallow soils (above 108 cm), despite the added parameters required. In
39   addition, this model is uniquely capable of reproducing transient CO_2 flux rates associated with
40   dynamic microbial response to changing soil moisture. In contrast, the first-order model achieves
41   better AIC scores when simulating the incubation data obtained from our deepest soils (112-165
42   cm). However, deep soils constitute a minor contribution to the overall CO_2 flux of an intact soil
43   column. Thus, the dormancy-incorporated model may better simulate respiration of the whole
44   soil.

45
46   **1. Introduction**
47   Soils are one of the largest reservoirs of terrestrial carbon at the Earth's surface and thus
48   represent a significant potential source of CO_2 to the atmosphere via heterotrophic and
49   autotrophic respiration (Batjes, 1996; Bellamy et al., 2005). Previous studies have shown a wide
50   variety of parameters can influence the rate of soil carbon respiration, for instance, temperature
51   (*e.g.* Lloyd and Taylor, 1994; Kirschbaum, 1995; Rey et al., 2005; Vanhala et al., 2008;
52   Niklińska and Klimek, 2007; Lellei-Kovács et al., 2016), microbial community composition (*e.g.*,
53   Monson et al., 2006; Cleveland et al., 2007; Li et al., 2006; Vanhala et al., 2005; Kant et al.,
54   2011), pH (e.g., Bååth and Anderson, 2003; Vanhala, 2002), soil organic carbon composition
55   (e.g., Cross and Sohi, 2011; Sanaullah et al., 2012), soil texture (e.g., Li et al., 2015), and soil
56   moisture (e.g., Orchard and Cook, 1983; Howard and Howard, 1993; Wagle and Kakani, 2014;
57   Jia et al., 2007).

58   Among these factors, the pronounced influence of water availability (soil moisture) on the rate at
59   which CO_2 is produced within soil profiles is of particular interest, as this relationship indicates a
60   direct feedback between the hydrologic cycle and the carbon cycle. Quantifying this relationship
61   is vital to the prediction of carbon cycle dynamics in a changing climate (Luo et al., 2016). Many
62   studies across a wide range of settings have demonstrated a positive correlation between soil
63   respiration rate and moisture in arid and semi-arid systems, and a negative correlation in soils
64   approaching saturation, with a peak in between (Davidson et al., 1998; Einola et al., 2007;
65   Elberling, 2003; Euskirchen et al., 2003; Falk et al., 2005; Grant and Rochette, 1994;
66   Grundmann et al., 1995; Hao et al., 2016; Harmon, 2009; Harmon et al., 2011; Howard and
67   Howard, 1993; Husen et al., 2014; Jin et al., 2008; Kang et al., 2003; Mielnick and Dugas, 2000;
68   Moncrieff and Fang, 1999; Pumpanen et al., 2003; Reichstein et al., 2003; Rey et al., 2005; Tian
69   et al., 2010; Verburg et al., 2005; Wang et al., 2010). When soils approach full water saturation,
70   pore wet-up and blockage combine to constrain the availability of oxygen by limiting the
71   diffusion rate (Cook and Knight, 2003; Grant and Rochette, 1994; Skopp et al., 1990), resulting
72   in diminished respiration across intact soil cores (Gabriel and Kellman, 2014). The factors

73 contributing to reduced respiration rates at low soil moisture contents are less clear. Two
74 processes have been suggested to describe this response. First, the availability of accessible bio-
75 available carbon indirectly affects microbial activity as a result of decreased water connectivity
76 as soil pores dry, which hinders the transport of dissolved organic matter and other nutrients
77 (Blazewicz et al., 2014; Davidson et al., 2014; Schjønning et al., 2003; Skopp et al., 1990).
78 Relatedly, some studies have suggested that the soil moisture-respiration relationship could stem
79 from decreased organic carbon addition to soils via root exudates in drier conditions (Canarini
80 and Dijkstra, 2015; Gorissen et al., 2004; Persson et al., 1995). The second process involves a
81 direct limitation on respiration rate as a result of dormancy triggered by a decrease in soil
82 moisture as a survival mechanism. Such a reduction of active microbial biomass capable of
83 respiration thus results in an overall slower metabolism and reduced soil carbon respiration rates
84 (Brockett et al., 2012; Lennon and Jones, 2011; Manzoni et al., 2014; Stevenson, 1977; Wang et
85 al., 2015).

86 The response of soil respiration rates to wetting events is also a transient feature. When soils are
87 rewet after a prolonged period of dry conditions, it is common to observe a large pulse of CO_2
88 followed by a decrease to lower, steady state values (Borken and Matzner, 2009; Inglima et al.,
89 2009; Kim et al., 2010; Wu and Lee, 2011). This observation is commonly referred to as the
90 Birch effect (Birch, 1958, 1960, 1964). The validity of the Birch effect has been suggested in
91 both controlled incubation (Göransson et al., 2013; Kieft et al., 1987; Shi and Marschner, 2014;
92 Unger et al., 2010) and field-scale systems (Cable et al., 2008; Xu et al., 2004; Yan et al., 2014).
93 A recent study by Fan et al. (2015) demonstrated that this initial pulse can represent a major
94 component of the total carbon respiration flux from soils, however, few models have the
95 availability to capture this behavior.

96 A wide variety of explanations for the Birch effect have been proposed. Among these, several
97 studies have suggested extra-cellular enzymes (exoenzymes) produced by microbes for the
98 purpose of solubilizing complex carbon to readily metabolized compounds remain active even in
99 dry conditions (Blankinship et al., 2014). As a result, low molecular weight carbon accumulates
100 during dry periods, leading to an initially high concentration when soil moisture rises again
101 (Iovieno and Bååth, 2008; Lawrence et al., 2009; Manzoni et al., 2014; Meisner et al., 2015;
102 Miller et al., 2005) and furthermore, a longer period of dry conditions results in the accumulation
103 of soluble carbon. Here, we implemented this mechanism in the modeling frameworks described
104 in Sect. 3 to capture dynamic behavior associated with the Birch effect.

105 In addition, different microbial communities exhibit unique optimal effective saturation ranges
106 (Barnard et al., 2013, 2015; Evans and Wallenstein, 2014; Lauber et al., 2013). This observation
107 implies, for example, that a microbial population which is active at a low soil moisture may be
108 dormant at higher moisture, leading to distinct activated microbial communities in the same soil
109 sample. Moreover, the rate of activation following a change in effective saturation is unique to
110 each microbial population (Blagodatskaya and Kuzyakov, 2013; Martiny et al., 2013; Placella et
111 al., 2012; Schimel and Schaeffer, 2015). This variation in response times derives from the
112 distinction between r- and K-strategies within the microbial community population (Andrews
113 and Harris, 1986; Dorodnikov et al., 2009), where the former have evolved to take advantage of
114 short term favorable conditions through rapid, energy inefficient population growth and the latter
115 subsist under less optimal conditions through slower productivity and increased efficiency.

116 In total, these studies illustrate a suite of complex and highly coupled relationships between the
117 hydrology, microbiology and carbon dynamics of soils. As a result, a wide variety of models

Biogeosciences
Discussions

118   have been developed for soil respiration as a function of soil moisture (Abramoff et al., 2017;
119   Chen et al., 2011; Hashimoto and Komatsu, 2006; Lawrence et al., 2009; Manzoni et al., 2012;
120   Moyano et al., 2012, 2013; Paul et al., 2003; Tian et al., 2010; Welsch and Hornberger, 2004).
121   These approaches have involved a broad diversity of structures in the effort to achieve a more
122   robust approach appropriate to a variety of soil types and locations. In particular, first-order
123   kinetic rate expressions featuring simplified parameterizations for soil carbon mineralization are
124   widely used in Earth system models, and have been successfully applied to simulate soil
125   respiration in some natural settings (Todd-Brown et al., 2013). Though the simplified parameter
126   set necessary for these functional forms is easily constrained by experimental datasets, and is
127   particularly necessary in cases where available data are limited, recent studies have shown that
128   such a simple model is not always able to explicitly demonstrate the transient changes
129   accompanied by variations in soil moisture (Lawrence et al., 2009). Recently, process-based
130   models relating respiration to moisture-dependent microbial functionality have been proposed
131   (Manzoni et al., 2014, 2016). These process-based modeling frameworks can dynamically
132   simulate soil respiration rate in changing moisture conditions, offering a promising approach for
133   extending model applications reliably across a range of conditions.-Thus, in dynamic systems
134   where transient pulses in CO_2 comprise a significant portion of the respiration flux (*e.g.* Fan et
135   al., 2015; Meisner et al., 2015), use of a more complex, process-based model for respiration rate
136   may be advantageous despite the cost of increased parameterization.

137   Therefore, we evaluated the performance of a process-based approach featuring a dormancy
138   model adapted from Manzoni et al. (2014), including the capacity to calculate the transition rates
139   between active and dormant microbial states as a function of soil moisture, in comparison to a
140   simpler first-order respiration model. Both models were calibrated using CO_2 respiration rates
141   obtained from a set of incubation experiments, using the shallow depth of a soil column collected
142   from the East River watershed located near Gothic, Colorado, USA. The calibrated models with
143   optimal parameter sets were then applied to each depth of the same soil profile, followed by a
144   quantitative evaluation of their relative fidelity using an Akaike Information Criterion (AIC)
145   method.

146
147   **2. Materials and methods**

148   2.1 Sample collection

149   Soil samples were collected in the upper East River watershed within the Gunnison River basin,
150   located near Crested Butte, Colorado, USA (Fig. 1). The upper East River is a high elevation
151   watershed with an average elevation of 3350 m. Stream flow is dominated by snowmelt in spring
152   and summer with the amount approximately equal to the total water demand (Markstrom and
153   Hay, 2009).

154   The sampling site for the current study is underlain by the calcareous shale from the Cretaceous
155   Mancos Shale Formation, with colluvial sediments at the surface, ~3.5 km north-west of Rocky
156   Mountain Biological Laboratory (RMBL). The predominant vegetation in this section of the
157   catchment is sub-alpine meadow. The sampling site has a seasonal drainage environment with
158   little or no slope, with an average annual temperature of 1 ºC and an average precipitation of 1.23
159   ± 0.26 m/year driven by both an annual monsoon season (~20 % of total precipitation) and as
160   snowfall (Winnick et al., 2017). Though precipitation predominantly occurs in the winter and
161   spring months, local soil moisture is significantly affected by summer rainfall (Harte et al., 1995).

162   Soil samples were collected in November, 2015 along Bradley Creek, a tributary of the East
163   River. Soil cores were taken at ~50 cm intervals from a hand-augered hole to a maximum depth
164   of 165 cm. After collection, samples were sealed in plastic bags and kept under cool, dark
165   conditions until processing could be completed. Prior to incubations, all soils were air-dried for
166   two weeks at ambient temperature (22 ºC) before crushed and sieved to 2 mm to remove the
167   coarse fraction, consisting of large stones and biological material.

168   2.2 Effective Saturation

169   Water holding capacity was determined by wetting three subsamples of air-dried soils gradually
170   until they became fully saturated. Samples were weighed before and after water addition to
171   quantify the mass needed for the soils to fully saturate for all three subsamples. The average of
172   the three numbers was used as the final saturated value with a standard deviation smaller than 5 %
173   of the water mass, where the air-dried samples are considered 0 % ($Sat_{residual}$), and 100 %
174   represents full saturation (Sat_{sat}). These values are subsequently reported as effective saturation
175   (Se, defined as $(Sat_{sample} - Sat_{residual})/(Sat_{sat} - Sat_{residual})$) for the remainder of the paper.

176   2.3 Soil Carbon Content

177   An elemental analyzer (EA) was used to determine the composition of carbon in the soils prior to
178   incubations. All EA measurements were performed using the Carlo-Erba NA 1500 analyzer (CE
179   Elantech, Inc., Lakewood, NJ, USA[*]) at the Environmental Measurements Facility (EM1) at
180   Stanford University. To measure the total carbon (TC) of the samples, 20-30 mg of ground soil
181   samples were weighed into tin capsules and loaded into the analyzer. A standard method was
182   used to measure total inorganic carbon (TIC) and total organic carbon (TOC) (Loeppert and
183   Suarez, 1996). Briefly, 400 mg of ground soil sample was added to a scintillation vial. Then 4
184   mL of 3M HCl$_{(aq)}$ was slowly added to the vial via a pipette to remove inorganic carbonate, and
185   the vial was capped loosely. The vial was swirled occasionally for 15 minutes and the cap was
186   removed to displace accumulated CO_2 until the weight of the vial stopped changing. The solution
187   was centrifuged to remove the supernatant, and the soil pellet was air-dried and ground with
188   agate mortar and pestle, then 20-30 mg of ground soil samples was weighed into tin capsules and
189   injected into the analyzer to measure the remaining TOC. TIC is the difference between TC and
190   TOC (Table 1). Three subsamples from each soil depth were measured for both TC and TOC to
191   test the accuracy and precision of the measurement (standard deviation shown in Table 1).

192   2.4 Soil incubations

193   Incubation vessels were constructed by drilling two holes in the caps of 948-ml glass canning
194   jars. Plastic bulkhead fittings (1/4-inch outer diameter) were installed in the holes with epoxy to
195   prevent gas leakage. Crack-resistant polyethylene tubing (1/4-inch outer diameter and 1/8-inch
196   inner diameter) was connected to both sides of the bulkheads and a plastic one-way value
197   attached to the external portion of the tubing to seal the chambers. Respiration was then
198   quantified by circulating the headspace in each jar into an LICOR-8100 Infrared Gas Analyzer
199   (Licor Biosciences, Lincoln, NE, USA[*]) to measure CO_2 concentration. During measurements,
200   the upper tube (closest to the cap) was attached to the inlet of LICOR-8100, and the lower tube
201   (close to the soil) was attached to the outlet to facilitate circulation.

---

[*] Any use of trade, firm, or product names is for descriptive purposes only and does not imply endorsement by the U.S. Government.

202   Incubation experiments were conducted by adding 75 grams of air-dried soil from three soil
203   depth intervals (0-52 cm, 63-108 cm, 112-165 cm) to the incubation vessels, subject to 4 distinct
204   *Se* values of 0, 33 %, 66 %, and 100 % by adding deionized water. All samples were initially
205   purged with CO_2 free air (zero air, SJ smith[*]) for over 10 times the size of the headspace and
206   kept under 22 degrees Celsius throughout the experiment. Incubations were run over a 10-day
207   period with daily sampling. After every analysis, the vessels were purged again with CO_2 free air
208   to reset the O_2 and CO_2 concentrations in the headspace. As a result, oxygen limitation to the
209   overall respiration rate is partially mitigated by the replenishment of the headspace, however
210   high fluid saturation levels in some of the experiments still support oxygen limited rates. All
211   respiration rates are calculated by measuring the CO_2 accumulated over the prior 24-hour
212   interval, and thus should be considered as the average respiration rate of the previous day (Table
213   2).

214
215   **3. Results**

216   The concentrations of TOC in each depth of the soil profile are given in Table 1. The results
217   show that TOC decreases with depth at all three sites, which is expected as organic inputs
218   associated with biological activities are most abundant at the surface and decline with depth. In
219   addition, the TIC also decreases with depth, suggesting that the highest carbonate concentration
220   occurs at a depth shallower than 52 cm at this sampling site. The TIC concentration is not further
221   discussed in the scope of this paper.

222   Respiration rates for all three soil depths at different effective saturations (*Se* = 0, 33 %, 66 %
223   and 100 %) for the first day of incubation show similar patterns across all depths (Fig. 2, Table
224   2), where respiration rates are positively correlated with effective saturation in dry conditions
225   and negatively correlated in wet conditions. The peak respiration rate for both the shallow and
226   intermediate depths lies around 66 % *Se* while the deepest depth displays a slight shift in
227   maximum value towards 33 % *Se*.

228   Respiration rates evolve with time in all three sampled depth intervals. This evolution is
229   illustrated for the shallow depth soil sample for the four effective saturation values (Fig. 3). All
230   respiration rates increase to a maximum value before decreasing to an apparent steady state, as is
231   typical of the Birch Effect. The time to reach peak respiration rate differs across the range of
232   effective saturations tested. At lower effective saturation (0 % and 33 %), the peak values appear
233   approximately 24 hours after initiation of the incubation, while at higher moisture content (66 %
234   and 100 %), this occurs approximately 48 hours after rewetting.

235   We note that no replicates were performed as a part of the incubation experiments due to sample
236   limitations, and there is certainly error associated with the measured rates. However, we note that
237   the respiration data adequately illustrate the expected trend as a function of both soil moisture
238   and time, which is the key point of the current study. Thus, we utilize the reported dataset in
239   order to calibrate the modeling approaches described below as a means of demonstrating their
240   capacity to reproduce commonly observed behavior.
241
242   **4. Model development**

243   For both models, the initial condition is generated to minimize the deviation of the model outputs
244   from incubation experiment measurements, and kept consistent while simulating different *Se*.
245   The sensitivity of the models to these initial conditions is explored further in Sect. 5.1.

246   4.1 First-order model

247   In the current and following sections, all flux rate and compartmental concentration units are in
248   gC m^{-3} soil/hour and gC m^{-3} soil, respectively, as in Manzoni et al. (2014).

249   In our 'first-order' model framework, organic carbon is categorized into three groups: substrate
250   carbon, soluble carbon, and biomass (Fig. 4a). Substrate carbon represents a complex carbon
251   form that cannot be directly accessed by microbial communities for respiration. Through a
252   solubilization process, this complex carbon is converted to soluble carbon, which is considered
253   bioavailable for respiration and production of CO_2. The solubilization rate is linearly dependent
254   on the amount of substrate carbon (Lawrence et al., 2009),

255
$$R_{sol,ij} = k_{sol,i} \times F_{Se,j} \times C_{sub,i} \tag{1}$$

256   where $R_{sol,i}$ is the concentration of soluble carbon (gC m^{-3}), $k_{sol,i}$ is the solubilization rate
257   constant (hour^{-1}), and $C_{sub,i}$ is the concentration of the substrate carbon (gC m^{-3}). $F_{Se,i}$ is a non-
258   dimensional factor constraining the solubilization and respiration rates based on Se (Eq. (2)). The
259   subscript i denotes a given subcategory of the total organic carbon (*e.g.* allowing consideration of
260   a range of recalcitrance), assuming different forms of substrate carbon will form into consistently
261   different forms of soluble carbon. Similarly, the subscript 'j' denotes different subcategories of
262   microbial communities that contribute to the solubilization of such substrate carbon.

263   The behavior of $F_{Se,j}$ is such that a sharp linear increase occurs as a function of Se up to a
264   threshold, $Se_{thres,j}$ followed by a parabolic decrease in respiration for values of Se above the
265   threshold until total saturation is reached (Gusman and Mariño, 1999; Cabon et al., 1991;
266   Porporato et al., 2003):

267
$$F_{Se,j} = \begin{cases} \frac{Se}{Se_{thres,j}}, & 0 \leq Se < Se_{thres,j} \\ \frac{Se_{thres,j}}{Se}, & Se_{thres,j} \leq Se \leq 1 \end{cases} \tag{2}$$

268   The threshold effective saturation is defined as the value of Se at which the respiration rate
269   reaches its maximum. Different $Se_{thres,j}$ have been applied to uptake pathways simulating the
270   distinct optimal Se for different microbial communities. An arbitrary choice of $Se_{thres,j} = 60\%$
271   is presented as an illustrative example of the behavior of this factor (Fig. 5).

272   Though this application of $F_{Se,j}$ in the solubilization rate expression is consistent with prior
273   studies (Lawrence et al., 2009; Parton et al., 1987), we note that this form of moisture constraint
274   is normally used to describe an exoenzyme rate control (Schimel and Weintraub, 2003), which is
275   not included in this modeling scheme. In addition, previous studies have shown that while the
276   use of this exoenzyme-catalyzed solubilization rate may be beneficial under certain rewetting
277   events, this approach often results in poor reproduction of constant moisture content behavior
278   relative to a simpler first-order solubilization rate (Lawrence et al. 2009). In that case, a direct
279   comparison of the two versions of the first-order model using different solubilization expressions
280   (Eq. (1) or (3)) is necessary (Fig. 6a, Table 3.):

281
$$R_{sol,i} = k_{sol,i} \times C_{sub,i} \tag{3}$$

282   The result explicitly shows that the respiration rate for the lower Se exceeds that for the high Se
283   after approximately 85 hours with application of Eq. (3), which contradicts the data. In addition,
284   we observe that the use of this expression does not influence the monotonic nature of the

285 respiration rate as a function of carbon availability. Thus, we conclude that Eq. (1) is superior for
286 the first-order model, and is used throughout the remainder of the paper.

287 The total microbial respiration rate (i.e. mineralization from soluble carbon to CO_2), U_{FO}, is
288 treated as the sum of a series of simple pseudo-first-order kinetic rate expressions with respect to
289 n subcategories of different soluble organic carbon classes:

290
$$U_{FO} = \sum_{i,j}^{n,m} k_{up,i} \times F_{Se,j} \times C_{soluble,i} \qquad (4)$$

291 where $k_{up,i}$ is the first-order maximum uptake rate constant (hour^{-1}), and $C_{soluble,i}$ is the
292 concentration of soluble carbon belonging to a given compositional subgroup (gC m^{-3}).

293 Net respired carbon is a result of two metabolic pathways: catabolic and anabolic. In the
294 catabolic pathway, soluble carbon is converted into CO_2 for energy production, while in the
295 anabolic pathway, it is assimilated by the microbes as new biomass, resulting in biomass growth
296 (Lawrence et al., 2009; Manzoni et al., 2014). In this first-order model, it is assumed that 90 % of
297 respired carbon is converted to CO_2, leaving the remaining 10 % for the anabolic growth
298 pathway.

299 Microbial turnover, including deceased and lysed microbial cells, are treated as a form of soluble
300 carbon and are thus bioavailable (Manzoni et al., 2014). The total mortality rate is considered the
301 sum of first-order functions of 'm' subcategories of living biomass (e.g. allowing consideration
302 of a range of response rates and optimal Se values) for different microbial subcategories:

303
$$RM = \sum_{j=1}^{m} k_{mor} \times Bio_j \qquad (5)$$

304 where RM is the amount of biomass that dies in a given time increment (gC m^{-3} hour^{-1}), k_{mor} is
305 the mortality rate constant (hour^{-1}), and Bio_j is the biomass concentration (gC m^{-3}). For
306 simplicity, we assume the mortality rate constant is identical for all microbial populations.

307 These series of equations were implemented in a commercial software package (Matlab Release
308 2016a, The MathWorks Inc., Natick, MA, 2016*). Simple mass balance equations are
309 implemented in combination with Eq. (1-2) and (4-5) to account for all inputs and outputs across
310 each carbon pool (Fig. 4a). For example, the substrate carbon pool is calculated as

311
$$C_{sub_{new}} = C_{sub_{old}} - R_{sol} \times \Delta t \qquad (6)$$

312 where Δt is the duration of each time step (hour).

313 The performances of the first-order model with a single microbial community and category of
314 organic carbon (m, n = 1, referred to as FO1), and two microbial communities along with two
315 subcategories of organic carbon (m, n = 1, referred to as FO2) are further evaluated in Sect. 5.1
316 and 5.2, respectively.

317 4.2 Dormancy model

318 The second model, which we refer to as the 'dormancy' model, is modified from the approach of
319 Manzoni et al. (2014) to allow for changes in the biomass in response to changes in effective
320 saturation. Within the dormancy model, the biomass pool is subdivided into two subcategories,

---

* Any use of trade, firm, or product names is for descriptive purposes only and does not imply endorsement by the
U.S. Government.

Biogeosciences
Discussions

321   active biomass and dormant biomass, with the other two carbon pools remaining the same (Fig.
322   4b), which avoids the uncertainty of an additional enzyme parameter ($Se_{thres,i}$) and poor
323   reproduction of constant moisture using Eq. (1) as noted by Lawrence et al. (2009). Thus we
324   proceed with a first-order solubilization rate (Eq. (3)) for the dormancy model. In doing so, the
325   solubilization process is assumed to be independent of shifts in the microbial biomass such that
326   enzyme activity is not a function of *Se*. This approach distinguishes the solubilization rate of the
327   dormancy model (Eq. (3)) from that of the first-order model (Eq. (1)) in that the former includes
328   a non-dimensional moisture scalar. However, we state that the solubilization rate express chosen
329   for each of the two models is optimal, ensuring the robustness of the comparison between the
330   two models.

331   Distinct from the first-order model described in Sect. 4.1, the total microbial respiration rate (U_D)
332   is treated here as a dual Monod rate law, which is a function of the amount of active biomass and
333   the availability of both O_2 and soluble carbon, allowing both soluble carbon and O_2 to be the
334   limiting factor in the reaction:

$$U_D = \sum_{i,j}^{n,m} k_{up,j} \times Bio_{active,j} \times \frac{C_{soluble,i}}{(C_{soluble,i}+C_{half,i})} \times \frac{O_{2(aq)}}{(O_{2(aq)}+K_{half})} \qquad (7)$$

336   where $k_{up,j}$ is the maximum uptake rate constant (hour^{-1}), $Bio_{active,j}$ is the concentration of
337   (active) biomass (gC m^{-3}), $C_{soluble,i}$ is the concentration of soluble carbon (gC m^{-3}), and $C_{half,i}$ is
338   the amount of soluble carbon where the uptake rate is 0.5 of the maximum value (also known as
339   the half saturation constant, gC m^{-3}). The subscripts *i* and *j* denote different subcategories of
340   soluble carbon and microbial communities respectively, similar to the first-order model, and the
341   superscripts *n* and *m* denote the quantity of soluble carbon and microbial community
342   subcategories respectively. The $O_{2(aq)}$ is dissolved oxygen concentration in water (gC m^{-3}) in
343   equilibrium with a specified partial pressure of O_2 (bar), and K_{half} is the half saturation constant
344   of the dissolved oxygen concentration (gC m^{-3}). Similar to the first-order model, 90 % of the
345   total respired carbon is converted to CO_2, leaving the remaining 10 % as anabolic growth. The
346   use of a dual Monod rate expression for the microbial respiration process allows both soluble
347   carbon and O_2 to be the limiting factor in the reaction.

348   We utilize a simplified version of the Manzoni et al. (2014) expressions for time-dependent rates
349   of microbial activation and dormancy. The rates of biomass activation and dormancy are
350   modeled as a function of *Se* with the following expressions:

$$Rate_{a \to d,j} = k_{tran,j} \times 1/(1 + (\frac{Se_{sample}}{Se_{half,j}})^b) \times Bio_{active,j} \qquad (8)$$

$$Rate_{d \to a,j} = k_{tran,j} \times 1/(a \times (\frac{Se_{half,j}}{Se_{sample}})^b + 1) \times Bio_{dormant,j} \qquad (9)$$

353   where Se_{sample} is effective saturation of the sample, and the variable $k_{tran,j}$ is the maximum
354   transition rate constant (hour^{-1}), while $Se_{half,j}$ is the saturation at which Eq. (8) is equal to
355   $0.5 \times k_{tran,j}$. Different $Se_{half,j}$ can be derived from the original form of Eq. (8) and (9), as in
356   Manzoni et al. (2014), assuming a constant ratio between the two values. Parameter '*a*' is used in
357   Eq. (9) to simplify the functional form by using the same $Se_{half,j}$ for both rates. The pore size
358   distribution parameter '*b*' is adjusted from the Brooks-Corey equation based on a water retention
359   curve. In this study, the *b* value employed by Manzoni et al. (2014) is used (Table 4).

360   Eq. (8) and (9) enable a time-dependent response in the transition between active and dormant
361   biomass to perturbations in effective saturation. The two competing rates represent different
362   amounts of biomass converting unidirectionally from $Bio_{active,j}$ to $Bio_{dormant,j}$ ($Rate_{a \rightarrow d,j}$) and
363   from $Bio_{dormant,j}$ to $Bio_{active,j}$ ($Rate_{d \rightarrow a,j}$), and this competition eventually stabilizes in a
364   balance between the two rates such that a dynamic equilibrium describes the population of both
365   active and dormant biomass. Microbial mortality is treated in the same manner utilized for the
366   first order model (Eq. (4)), with distinct mortality rate constants assigned for active and dormant
367   biomass (referred to as k_{mor-a} for active biomass, and k_{mor-d} for dormant biomass).

368   An example of this behavior is provided in Fig. 7. This example illustrates the characteristic
369   response to a wetting event, which replaces the static treatment used in Eq. (4), and the time
370   scale over which equilibrium is reestablished for an assumed rate constant of 1 hour^{-1}. All the
371   parameters used in this simulation are reported in Table 4.

372   As with the first order model described previously, the performance of the dormancy model with
373   a single microbial community and category of organic carbon (m, n = 1, referred to as DM1), and
374   two microbial communities along with two subcategories of organic carbon (m, n = 1, referred to
375   as DM2) are further evaluated in Sect. 5.1 and 5.2, respectively.

376

377   **5. Discussion**

378   5.1 FO1 and DM1 application to incubation data

379   The FO1 model was applied to the incubation experimental results described in Sect. 3, where
380   the time series data for 66 % and 33 % Se from the shallow soil depth were used as a base case
381   (Fig. 6a). The results show reasonable agreement with the data, however, in this simplified
382   approach, respiration rate is only capable of monotonic decrease (if the initial $R_{sol} < U_{FO}$), or
383   increase (if the initial $R_{sol} > U_{FO}$) due to the first order dependence on carbon concentration. As
384   a result, the model is not capable of accurately representing the transient increase in respiration
385   rate initially observed following a rewetting event (i.e. the Birch effect).

386   Similarly, DM1 was applied to the incubation results for 66 % Se as a base case. We observed a
387   significant improvement in model representation of the transient changes in CO_2 respiration rate
388   accompanied by the rewetting event at early time (Fig. 8) with comparable parameter values
389   (Table 4). The transition of the biomass from an initially fully dormant state to predominantly
390   active was triggered by the instantaneous increase in Se from 0 to 66 % at the start of the
391   simulation. A lagged response in respiration rate was presented following this instantaneous
392   rewetting, which successfully simulated the experimental data. With further time, the initially
393   rapid rate of CO_2 production decreases as the excess soluble carbon initially available is depleted.
394   Ultimately, the rate of soluble carbon consumption (Eq. (7)) decreases to a value which is
395   balanced by the rate of substrate carbon solubilization (Eq. (3)) and the system approaches a
396   steady state. Oxygen concentration was treated as a constant rather than a limiting factor in this
397   model, assuming that the periodic replenishment of O_2 implemented in our incubation
398   experiments was sufficient to compensate for consumption due to aerobic respiration. It is not
399   surprising that DM1 is capable of generating more accurate results than FO1 with the extra
400   flexibility provided by the additional parameters. The extent to which improved accuracy is
401   offset by the additional parameters is further considered in a subsequent section (Sect. 5.3).

402 The initial condition of a simulation obviously exerts a substantial impact on any transient model
403 output. In the current approach, the starting concentrations of different carbon pools are poorly
404 constrained and thus a model sensitivity analysis is provided. The simulations assume a
405 reasonable assumption for the value of initial soluble carbon concentration (Tables 3 & 4), and
406 include a ±20 % variation (80 % to 120 %) to illustrate sensitivity for all four models considered
407 in this paper (FO1, FO2, DM1 and DM2). Although the predicted respiration rates are positively
408 correlated with the initial soluble carbon concentration, this variation gradually fades away as
409 respiration approaches steady state, where the rate of soluble carbon consumption through
410 respiration is balanced by the dissolution of substrate carbon.

411 To capture the dynamic response of soil respiration to variable Se, it is critical that the parameter
412 values used in DM1 are generally applicable across the depth profile of the East River soils.
413 Model fidelity is tested by applying the same parameter values calibrated based on the 66 % Se
414 shallow soil sample datasets to the values obtained at 33 % Se (Fig. 8). The results clearly
415 indicate that this parameterization is unable to reproduce comparable results across a range of
416 saturations. Even though the modeled 33 % Se peak value generally agrees with incubation data,
417 which is lower than that of 66 % Se due to the lower fraction of active biomass, the model results
418 in a slower activation of dormant biomass which retards the time to peak respiration in
419 comparison to the measured data. The two more complex models (FO2 and DM2) are further
420 evaluated in the following section (Sect. 5.2).

421 5.2 FO2 and DM2 application to incubation data

422 To improve upon the base case scenario during the transient period following a rewetting event,
423 FO2 and DM2 were tested in a manner similar to the procedure described for FO1 and DM1.
424 Two distinct microbial populations (m = 2) were assumed to exist in the soil samples: an r-
425 selection population, capable of activating rapidly after rewetting, and a K-selection population
426 subject to a longer transient activation period. In addition, the substrate and soluble organic
427 carbon pools were also subcategorized into labile and recalcitrant subcomponents. The models
428 were parameterized such that the r-selection microbial category is more adaptable to dynamic
429 environments. This includes a faster activation rate at lower Se and a higher mineralization rate
430 constant for labile organic carbon, however, these r-strategists were assumed to have negligible
431 capacity to mineralize recalcitrant carbon. In contrast, the K-selection microbial subcategory is
432 characterized by a slower response time with the capacity to utilize both labile and recalcitrant
433 carbon. These differences in rate between the two microbial pools were achieved in the model by
434 variations in $k_{sol,i}$ (Eq. (1) and (3)), $Se_{thres,j}$ (Eq. (2)), and $k_{up,i}$ (Eq. (4), Table 3). Despite this
435 additional complexity, the model performance for FO2 was not improved compared to FO1 (Fig.
436 6b). Based on these results, we conclude that the monotonic trend in CO_2 respiration rate
437 produced by such a first-order approach is largely unaffected by both the extent to which the
438 carbon pools are subdivided into a range of reactivity, and the extent to which the microbial
439 communities are subdivided in terms of both carbon utilization efficiency and moisture-
440 dependent activation rate. Thus, FO1 is considered more efficient for the first-order approach,
441 and is utilized throughout this paper as a comparison to the dormancy model.

442 Because the principle disparity between the dormancy model and the observed trends is the clear
443 difference in timing of peak CO_2 production between the 33 % and 66 % Se experiments, a
444 similar approach was taken in applying two microbial communities (m = 2) with distinct
445 parameter values as in FO2. The sensitivity of DM1 to differences in $Se_{half,j}$ and $k_{up,j}$ is

446 illustrated (Fig. 9a and 9b) for a range of values is first checked while holding all other
447 parameters constant (Table 4, Se_{sample} set to 0.7). A lower $Se_{half,j}$ value results in faster
448 activation of dormant biomass (Eq. (9)) and slower dormancy of active biomass (Eq. (8)), while
449 a larger $k_{up,j}$ value induces more CO_2 produced in one time step (higher peak value) leaving less
450 available soluble carbon in the system. Accordingly, a lower $Se_{half,j}$ and larger $k_{up,j}$ result in a
451 more rapid increase in the respiration rate following rewetting, illustrated by an earlier time of
452 peak CO_2 production with a higher peak value, leaving less available soluble carbon in the
453 system, and thus an earlier decrease to steady state rates. Though the model sensitivity to the
454 $Se_{half,j}$ and $k_{up,j}$ parameters are comparable, we note that the $Se_{half,j}$ parameter alters the point
455 of dynamic equilibrium between the active and dormant biomass, while $k_{up,j}$ changes the rate of
456 microbial uptake regardless of the balance between the two biomass forms.

457 Though in principle we are expanding the dormancy model in the same manner as we did for the
458 first-order simulation, in practice the complexity with which activation rates are treated in the
459 dormancy-based approach requires further consideration of how multiple biomass sub-
460 communities should be implemented. Specifically, if optimal Se conditions support the rapid
461 activation of a given microbial population, then it follows that unfavorable Se conditions can
462 inhibit a given community (Barnard et al., 2013, 2015). This inhibition was not included in the
463 first-order model with two microbial communities (m = 2) in that it is fundamentally a limiting
464 factor of respiration rate, which cannot change the monotonic trend induced by the first-order
465 kinetics. In contrast, such inhibition is vital in the dormancy kinetics and should significantly
466 alter the peak height and position of the simulation. In order to impose this constraint on the
467 rapidly activating portion of the biomass in the current model, an additional Se dependent
468 inhibition factor is added to Eq. (7) specifically for the two types of microbial populations j,
469 representing r- and K-strategists, and two types of organic carbon subcategories i, representing
470 labile and recalcitrant components:

471 $$U_{i=lab,j=r} = k_{up,r} \times Bio_{active,r} \times \frac{C_{sol,lab}}{(C_{sol,lab}+C_{half,lab})} \times \frac{O_{2(aq)}}{(O_{2(aq)}+K_{half})} \times \left(\frac{1-(2Se_{sample}-1)^{1/3}}{2}\right) \quad (10)$$

472 and

473 $$U_{i=rec,j=K} = k_{up,K} \times Bio_{active,K} \times \frac{C_{sol,rec}}{(C_{sol,rec}+C_{half,rec})} \times \frac{O_{2(aq)}}{(O_{2(aq)}+K_{half})} \times \left(\frac{(2Se_{sample}-1)^{1/3}+1}{2}\right) \quad (11)$$

474 $k_{up,r}$ and $k_{up,K}$ are maximum uptake rate constants (hour^{-1}) specific to the $Bio_{active,r}$ and
475 $Bio_{active,K}$ subpopulations, respectively (Table 4). Furthermore, the r-selection biomass is
476 assigned an $Se_{half} = 0.25$ so that it is capable of activation at lower Se with $k_{tran} = 1$ (fast
477 activation, Eq. (8) and (9), [time^{-1}]), while the K-selection biomass is assigned an $Se_{half} = 0.55$,
478 thus restraining its activity under lower Se, with $k_{tran,j} = 1/60$ (slow activation, Eq. (8) and (9),
479 [time^{-1}]).

480 This form of inhibition is chosen because the functions provide valid numbers across the full
481 range of Se values. Moreover, this functional form returns a value of 1 when $Se = 100$ % and 0
482 when $Se = 0$ for K-selection biomass, thus limiting the respiration rates at lower Se values for the
483 K-selection biomass, with a gradient at intermediate values. Meanwhile, the opposite behavior is
484 specified for the r-selection biomass, thus limiting their respiration capability at higher Se values
485 (Fig. 10).

Biogeosciences
Discussions

486 Employing this adjusted version of the model (DM2), we again tested the ability to reproduce the
487 respiration datasets corresponding to multiple *Se* values for a common soil sample after
488 calibration (Fig. 11a). Incubation results for 100 % *Se* were absent in this simulation since our
489 modeling approach included a constant O_2 concentration, which contradicts the experimental
490 condition where O_2 is limited in the pore space at 100 % *Se*. DM2 shows clear improvement in
491 simulating soil respiration data with a single parameter set (Table 4) across a range of *Se*. Both
492 shallow and intermediate depth soil sample results are accurately reproduced by the model (Fig.
493 11b, 11c, Table 4), where the only difference in parameter values differentiating the two sets of
494 simulations is the amount of starting substrate carbon based on the EA results (Table 1). The
495 model somewhat over-predicts the respiration rate of deep soil samples. This may result from
496 chronic oxygen limitation at these depths (112-165 cm) in the field, thus leading to a distinct
497 microbial community more suited to suboxic conditions (Arora et al., 2016; Long et al., 2015).

498 5.3 Model precision vs. cost

499 Cubic interpolation was used to estimate the rate between incubation data points, allowing us to
500 integrate both the model output and incubation data through time (Fig. 12a). The resulting
501 cumulative CO_2 as a function of time estimated by both FO1 and DM2 was then compared
502 against incubation data (Fig. 12b) to quantitatively assess the accuracy of each simulation. Even
503 though both models over-predicted the cumulative CO_2 concentration, we observed that FO1
504 showed a relatively large over-prediction of the amount of CO_2 produced in response to a
505 wetting event. This relatively large over-prediction by the first-order model was due to the
506 disparity between the predicted high respiration rate resulting from the monotonic drop and the
507 low respiration rate observed at early time. In comparison, DM2 showed much better agreement
508 to the data for the first ~100 hours, illustrating a better performance with variable *Se*. The ratio of
509 integrated CO_2 concentration between the incubation data and outputs from the two models
510 illustrate the relative performance of the two approaches (Fig. 12c). Since the interpolated rates
511 from incubation experiments are consistently lower than outputs from both models (Fig. 12b),
512 the ratio of incubation/model CO_2 values fall between 0 and 1 (Fig. 12c), where lower values
513 indicate poorer agreement with the experimental data, and 1 indicates an exact match. This
514 exercise demonstrates that the ratio of FO1 is consistently lower than that of DM2 for all times
515 less than 100 hours, indicating that the first-order model cannot accurately simulate the transient
516 changes in respiration rate after soil is rewet (i.e. the Birch effect). After approximately 100
517 hours, both models establish close agreement to the data (ratio of integrated CO_2 ~0.9), meaning
518 they are equally accurate at steady state respiration. Thus, in general, the dormancy modeling
519 approach is necessary for accurate representation of dynamic responses to changing *Se* over short
520 timescales, such as in our incubation experiments, with the implementation of a dynamic
521 biomass activation process.

522 However, we recognize that additional parameterization increases the accuracy of a model at the
523 expense of both computational efficiency and parameter constraint. Thus, the Akaike
524 Information Criterion (referred to as AIC, Akaike, 1998), which takes both the number of
525 parameters and the goodness of fit into consideration, was applied to score the two models. The
526 Residual Sum of Squares (RSS) was calculated between incubation data and model output for
527 three depths of soil samples under 33 % and 66 % *Se* as follows,

528
$$RSS = \sum_{k=1}^{p}(MO_k - In_k)^2 \qquad (12)$$

529   where MO_k is the model output and In_k is the incubation data. The subscript 'k' denotes
530   different data points in a given depth and *Se*, and the superscript 'p' represents the total quantity
531   of data points.

532   While RSS values illustrate the goodness of fit for the two models, the number of parameters is
533   included in the AIC calculation as,

534    $$AIC = n \log(RSS/n) + 2l \qquad (13)$$

535   where *n* and *l* represent the number of data points and the number of parameters respectively.
536   The AIC value of the two models are listed in Table 5.

537   The results of these model-data comparisons show that the dormancy model not only achieves
538   higher accuracy while simulating the Birch effect, but obtains a lower AIC value with soils
539   above the 108 cm depth interval, indicating that this improvement outweighs the extra cost and
540   uncertainty accompanied by the increased model complexity. In contrast, the performance of the
541   first-order model appears superior according to its AIC value in simulating the deepest soils at
542   66 % *Se*.

543   We note that the deep-soil component of this sample set corresponds to approximately 13 % of
544   the total respiration taken over the shallow, middle and deep depths. Thus, in the scope of our
545   study, we conclude that DM2 will serve as a better tool in predicting the CO_2 flux of a whole soil
546   profile in most circumstances. Moreover, recent studies have demonstrated that Birch effects of
547   this nature can last over the duration of weeks to months and in some ecosystems they may
548   produce over 50 % of the total respired CO_2 (Fan et al., 2015). The inability to capture this Birch
549   dynamic in the first-order framework may generate even larger errors under environmentally
550   relevant conditions, indicating that application of DM2 is cost effective and necessary in
551   simulating environments where Birch effects are essential, especially where long periodicity is
552   expected.

553   In addition, we note that though the deep soil organic carbon concentration is relatively small
554   compared to shallow depths, and contributes less than 13 % of the total respiration, in total this
555   deep soil storage constitutes a significant terrestrial organic carbon stock across a broad diversity
556   of environments. This in turn represents a potentially significant source of atmospheric CO_2 if
557   such carbon were to become mobilized or otherwise biologically available (e.g. disturbances
558   (Trumbore, 2009)). Previous studies have employed a diversity of methods, including
559   radiocarbon dating (^{14}C), near edge X-ray absorption fine structure (NEXAFS) spectrometry, and
560   differential scanning calorimetry (DSC), to explore the chemical properties and stabilization
561   pathways of deep-soil organic carbon (Kleber et al., 2011). However, detailed modeling
562   approaches predicting the behavior of the deep-soil organic carbon are sparse. The results of this
563   model comparison suggest that respiration of deep-soil carbon in our samples is appropriately
564   modeled with a simplified first-order rate law rather than the dormancy rate law under conditions
565   analogous to rapid surface exposure, though this is based on a limited dataset and requires further
566   constraint. This difference may be related to more stable, high moisture *in-situ* conditions,
567   resulting in a dominant microbial community insensitive to moisture variation.

568   5.4 Future directions

569   Another potentially significant factor is the timespan over which *Se* changes during a wetting or
570   drying event. Shifts in the *Se* values in the current study were implemented as an instantaneous
571   change from 0 to a certain value at the beginning of the incubation. Though this is valid for the

Biogeosciences
Discussions

572 present experimental design, a gradual increase of Se from low to high is commonly observed in
573 reality as the result of extended and compounding periods of precipitation and dry out (Borken et
574 al., 2003). Based on the equations developed herein, we note that such a time-dependent change
575 in Se can support a transient increase in respiration rate using the first-order model (i.e. the
576 monotonic nature shown here would be alleviated). However, this would still omit the lagged
577 respiration peak generated using the dormancy model. Such cases require further testing, as
578 would be provided by a direct comparison of the performance of two models simulating one
579 identical dataset from *in situ* measurements over multiple precipitation events. This will be
580 addressed in subsequent studies using the East River Watershed datasets.

581 Finally, before applying the two models to *in situ* measurements, we recognize that the effects of
582 transport limitation are vital, and still missing from the current laboratory-based study, even
583 though the dormancy modeling approach can in theory provide soil respiration predictions in
584 dynamic hydrologic settings. In particular, a fixed O_2 concentration is set throughout the
585 simulations, assuming O_2 is never a limiting factor, yet clearly some contribution from oxygen
586 limitation at high Se values is demonstrated in the data. While this effect is minor in the current
587 experimental conditions, in natural environments, respiration can be limited by low O_2
588 concentration resulting from low replenishment rates at high Se (Eq. (9) and (10)) in that gas
589 diffusion is negatively correlated with Se (Pingintha et al., 2010). Under these conditions, our
590 current model could potentially over-estimate the respiration rate. Thus, an important expansion
591 of the process-based dormancy modeling approach (Eq. (6-10)) will be integration into a
592 reactive-transport modeling framework capable of linking the reaction network to gas and fluid
593 phase transport across intact soil columns.

594

595 **6. Conclusion**

596 Our incubation results show a positive correlation between CO_2 respiration rate and Se under dry
597 conditions and a negative correlation when soils approach saturation, similar to previous studies.
598 Dynamic shifts of soil respiration rates accompanied by dry-wet cycles (i.e. the Birch effect) are
599 also found in the incubation experiments with distinct peak heights and positions at different Se
600 values. An adjusted form of the reaction network developed by Manzoni et al. (2014), referred to
601 as the dormancy model, was built and compared against a widely-applied first-order model by
602 evaluating their performances in simulating the experimental data. With an adjustment that
603 allows the activation of unique microbial communities at distinct effective saturations, DM2
604 displays a better representation of the data, particularly in simulating temporal patterns of the
605 Birch effects. After evaluating both FO1 and DM2 with consideration of the quantity of
606 parameters, we conclude that despite the better performance of FO1 while simulating the
607 decomposition of deep soil organic carbon, the implementation of moisture-dependent activation
608 and dormancy rates provides an improved means of quantifying and predicting soil carbon
609 respiration of a soil column under dynamic hydrologic conditions.

610 Because soil organic carbon is a significant potential source of CO_2 to the atmosphere, this
611 improved simulation accuracy provides a better estimation of the budget of soil respired CO_2,
612 which can potentially be further utilized to constrain terrestrial carbon fluxes. Finally, we note
613 that the implementation of the current reaction network to a reactive-transport framework is
614 necessary and holds the potential to provide notably improved performance in the simulation of
615 soil carbon respiration across intact cores.

Biogeosciences
Discussions

Open Access

EGU

616

7. Competing interests

618 The authors declare that they have no conflict of interest.

619

8. Acknowledgments

626

Biogeosciences
Discussions

Open Access

EGU

627   References:

628   A. Jake Gusman, Miguel A. Mariño, 1999. Analytical Modeling of Nitrogen Dynamics in Soils
629   and Ground Water. Journal of Irrigation and Drainage Engineering 125, 330–337.
630   doi:10.1061/(ASCE)0733-9437(1999)125:6(330)
631   Abramoff, R.Z., Davidson, E.A., Finzi, A.C., 2017. A parsimonious modular approach to
632   building a mechanistic belowground carbon and nitrogen model. Journal of Geophysical
633   Research: Biogeosciences 122, 2418–2434. doi:10.1002/2017JG003796
634   Akaike, H., 1998. Information Theory and an Extension of the Maximum Likelihood Principle,
635   in: Parzen, E., Tanabe, K., Kitagawa, G. (Eds.), Selected Papers of Hirotugu Akaike.
636   Springer New York, New York, NY, pp. 199–213. doi:10.1007/978-1-4612-1694-0_15
637   Andrews, J.H., Harris, R.F., 1986. r- and K-Selection and Microbial Ecology, in: Marshall, K.C.
638   (Ed.), Advances in Microbial Ecology. Springer US, Boston, MA, pp. 99–147.
639   doi:10.1007/978-1-4757-0611-6_3
640   Arora, B., Spycher, N.F., Steefel, C.I., Molins, S., Bill, M., Conrad, M.E., Dong, W.,
641   Faybishenko, B., Tokunaga, T.K., Wan, J., Williams, K.H., Yabusaki, S.B., 2016.
642   Influence of hydrological, biogeochemical and temperature transients on subsurface
643   carbon fluxes in a flood plain environment. Biogeochemistry 127, 367–396.
644   doi:10.1007/s10533-016-0186-8
645   Bååth, E., Anderson, T.-H., 2003. Comparison of soil fungal/bacterial ratios in a pH gradient
646   using physiological and PLFA-based techniques. Soil Biology and Biochemistry 35, 955–
647   963. doi:10.1016/S0038-0717(03)00154-8
648   Barnard, R.L., Osborne, C.A., Firestone, M.K., 2015. Changing precipitation pattern alters soil
649   microbial community response to wet-up under a Mediterranean-type climate. ISME
650   Journal 9, 946–957. doi:10.1038/ismej.2014.192
651   Barnard, R.L., Osborne, C.A., Firestone, M.K., 2013. Responses of soil bacterial and fungal
652   communities to extreme desiccation and rewetting. ISME J 7, 2229–2241.
653   Batjes, N.H., 1996. Total carbon and nitrogen in the soils of the world. European Journal of Soil
654   Science 47, 151–163.
655   Bellamy, P.H., Loveland, P.J., Bradley, R.I., Lark, R.M., Kirk, G.J.D., 2005. Carbon losses from
656   all soils across England and Wales 1978-2003. Nature 437, 245–248.
657   doi:10.1038/nature04038
658   Birch, H.F., 1964. Mineralisation of plant nitrogen following alternate wet and dry conditions.
659   Plant and Soil 20, 43–49. doi:10.1007/BF01378096
660   Birch, H.F., 1960. Nitrification in soils after different periods of dryness. Plant and Soil 12, 81–
661   96. doi:10.1007/BF01377763
662   Birch, H.F., 1958. Pattern of Humus Decomposition in East African Soils. Nature 181, 788–788.
663   doi:10.1038/181788a0
664   Blagodatskaya, E., Kuzyakov, Y., 2013. Active microorganisms in soil: Critical review of
665   estimation criteria and approaches. Soil Biology and Biochemistry 67, 192–211.
666   doi:10.1016/j.soilbio.2013.08.024
667   Blankinship, J.C., Becerra, C.A., Schaeffer, S.M., Schimel, J.P., 2014. Separating cellular
668   metabolism from exoenzyme activity in soil organic matter decomposition. Soil Biology
669   and Biochemistry 71, 68–75. doi:10.1016/j.soilbio.2014.01.010
670   Blazewicz, S.J., Schwartz, E., Firestone, M.K., 2014. Growth and death of bacteria and fungi
671   underlie rainfall-induced carbon dioxide pulses from seasonally dried soil. Ecology 95,
672   1162–1172. doi:10.1890/13-1031.1

673 Borken, W., Davidson, E.A., Savage, K., Gaudinski, J., Trumbore, S.E., 2003. Drying and
674   Wetting Effects on Carbon Dioxide Release from Organic Horizons. Soil Science Society
675   of America Journal 67, 1888–1896. doi:10.2136/sssaj2003.1888
676 Borken, W., Matzner, E., 2009. Reappraisal of drying and wetting effects on C and N
677   mineralization and fluxes in soils. Global Change Biology 15, 808–824.
678   doi:10.1111/j.1365-2486.2008.01681.x
679 Brockett, B.F.T., Prescott, C.E., Grayston, S.J., 2012. Soil moisture is the major factor
680   influencing microbial community structure and enzyme activities across seven
681   biogeoclimatic zones in western Canada. Soil Biology and Biochemistry 44, 9–20.
682   doi:10.1016/j.soilbio.2011.09.003
683 Cable, J.M., Ogle, K., Williams, D.G., Weltzin, J.F., Huxman, T.E., 2008. Soil Texture Drives
684   Responses of Soil Respiration to Precipitation Pulses in the Sonoran Desert: Implications
685   for Climate Change. Ecosystems 11, 961–979. doi:10.1007/s10021-008-9172-x
686 Cabon, F., Girard, G., Ledoux, E., 1991. Modelling of the nitrogen cycle in farm land areas, in:
687   Groot, J.J.R., De Willigen, P., Verberne, E.L.J. (Eds.), Nitrogen Turnover in the Soil-
688   Crop System: Modelling of Biological Transformations, Transport of Nitrogen and
689   Nitrogen Use Efficiency. Proceedings of a Workshop Held at the Institute for Soil
690   Fertility Research, Haren, The Netherlands, 5–6 June 1990. Springer Netherlands,
691   Dordrecht, pp. 161–169. doi:10.1007/978-94-011-3434-7_3
692 Canarini, A., Dijkstra, F.A., 2015. Dry-rewetting cycles regulate wheat carbon rhizodeposition,
693   stabilization and nitrogen cycling. Soil Biology and Biochemistry 81, 195–203.
694   doi:10.1016/j.soilbio.2014.11.014
695 Chen, X., Post, W.M., Norby, R.J., Classen, A.T., 2011. Modeling soil respiration and variations
696   in source components using a multi-factor global climate change experiment. Climatic
697   Change 107, 459–480. doi:10.1007/s10584-010-9942-2
698 Cleveland, C.C., Nemergut, D.R., Schmidt, S.K., Townsend, A.R., 2007. Increases in soil
699   respiration following labile carbon additions linked to rapid shifts in soil microbial
700   community composition. Biogeochemistry 82, 229–240. doi:10.1007/s10533-006-9065-z
701 Cook, F.J., Knight, J.H., 2003. Oxygen transport to plant roots: Modeling for physical
702   understanding of soil aeration. Soil Science Society of America Journal 67, 20–31.
703 Cook, F.J., Thomas, S.M., Kelliher, F.M., Whitehead, D., 1998. A model of one-dimensional
704   steady-state carbon dioxide diffusion from soil. Ecological Modelling 109, 155–164.
705   doi:10.1016/S0304-3800(98)00034-9
706 Cross, A., Sohi, S.P., 2011. The priming potential of biochar products in relation to labile carbon
707   contents and soil organic matter status. Soil Biology and Biochemistry 43, 2127–2134.
708   doi:10.1016/j.soilbio.2011.06.016
709 Davidson, E.A., Belk, E., Boone, R.D., 1998. Soil water content and temperature as independent
710   or confounded factors controlling soil respiration in a temperate mixed hardwood forest.
711   Global Change Biology 4, 217–227. doi:10.1046/j.1365-2486.1998.00128.x
712 Davidson, E.A., Savage, K.E., Finzi, A.C., 2014. A big-microsite framework for soil carbon
713   modeling. Global Change Biology 20, 3610–3620. doi:10.1111/gcb.12718
714 Dorodnikov, M., Blagodatskaya, E., Blagodatsky, S., Fangmeier, A., Kuzyakov, Y., 2009.
715   Stimulation of r - vs. K -selected microorganisms by elevated atmospheric CO_2 depends
716   on soil aggregate size. FEMS Microbiology Ecology 69, 43–52. doi:10.1111/j.1574-
717   6941.2009.00697.x

718 Einola, J.-K.M., Kettunen, R.H., Rintala, J.A., 2007. Responses of methane oxidation to
719   temperature and water content in cover soil of a boreal landfill. Soil Biology and
720   Biochemistry 39, 1156–1164. doi:10.1016/j.soilbio.2006.12.022
721 Elberling, B., 2003. Seasonal trends of soil CO2 dynamics in a soil subject to freezing. Journal of
722   Hydrology 276, 159–175. doi:10.1016/S0022-1694(03)00067-2
723 Euskirchen, E.S., Chen, J., Gustafson, E.J., Ma, S., 2003. Soil Respiration at Dominant Patch
724   Types within a Managed Northern Wisconsin Landscape. Ecosystems 6, 595–607.
725   doi:10.1007/PL00021505
726 Evans, S.E., Wallenstein, M.D., 2014. Climate change alters ecological strategies of soil bacteria.
727   Ecology Letters 17, 155–164. doi:10.1111/ele.12206
728 Falk, M., Paw U, K.T., Wharton, S., Schroeder, M., 2005. Is soil respiration a major contributor
729   to the carbon budget within a Pacific Northwest old-growth forest? Agricultural and
730   Forest Meteorology 135, 269–283. doi:10.1016/j.agrformet.2005.12.005
731 Fan, Z., Neff, J.C., Hanan, N.P., 2015. Modeling pulsed soil respiration in an African savanna
732   ecosystem. Agricultural and Forest Meteorology 200, 282–292.
733   doi:10.1016/j.agrformet.2014.10.009
734 Franzluebbers, A.J., 1999. Microbial activity in response to water-filled pore space of variably
735   eroded southern Piedmont soils. Applied Soil Ecology 11, 91–101. doi:10.1016/S0929-
736   1393(98)00128-0
737 Gabriel, C.-E., Kellman, L., 2014. Investigating the role of moisture as an environmental
738   constraint in the decomposition of shallow and deep mineral soil organic matter of a
739   temperate coniferous soil. Soil Biology and Biochemistry 68, 373–384.
740   doi:10.1016/j.soilbio.2013.10.009
741 Göransson, H., Godbold, D.L., Jones, D.L., Rousk, J., 2013. Bacterial growth and respiration
742   responses upon rewetting dry forest soils: Impact of drought-legacy. Soil Biology and
743   Biochemistry 57, 477–486. doi:10.1016/j.soilbio.2012.08.031
744 Gorissen, A., Tietema, A., Joosten, N.N., Estiarte, M., Peñuelas, J., Sowerby, A., Emmett, B.A.,
745   Beier, C., 2004. Climate Change Affects Carbon Allocation to the Soil in Shrublands.
746   Ecosystems 7, 650–661. doi:10.1007/s10021-004-0218-4
747 Grant, R.F., Rochette, P., 1994. Soil Microbial Respiration at Different Water Potentials and
748   Temperatures: Theory and Mathematical Modeling. Soil Science Society of America
749   Journal 58, 1681–1690. doi:10.2136/sssaj1994.03615995005800060015x
750 Grundmann, G.L., Renault, P., Rosso, L., Bardin, R., 1995. Differential Effects of Soil Water
751   Content and Temperature on Nitrification and Aeration. Soil Science Society of America
752   Journal 59, 1342–1349. doi:10.2136/sssaj1995.03615995005900050021x
753 Hao, Y., Nianpeng, H., Shenggong, L., Guirui, Y., Yang, G., Ruomeng, W., 2016. Impact of
754   Land Cover on Temperature and Moisture Sensitivity of Soil Organic Matter
755   Mineralization in Subtropical Southeastern China. Journal of Resources and Ecology 7,
756   85–91. doi:10.5814/j.issn.1674-764x.2016.02.002
757 Harmon, M.E., 2009. Woody Detritus its Contribution to Carbon Dynamics of Old-Growth
758   Forests: the Temporal Context, in: Wirth, C., Gleixner, G., Heimann, M. (Eds.), Old-
759   Growth Forests: Function, Fate and Value. Springer Berlin Heidelberg, Berlin,
760   Heidelberg, pp. 159–190.
761 Harmon, M.E., Bond-Lamberty, B., Tang, J., Vargas, R., 2011. Heterotrophic respiration in
762   disturbed forests: A review with examples from North America. Journal of Geophysical
763   Research: Biogeosciences 116, n/a-n/a. doi:10.1029/2010JG001495

764   Harte, J., Torn, M.S., Chang, F.-R., Feifarek, B., Kinzig, A.P., Shaw, R., Shen, K., 1995. Global
765   Warming and Soil Microclimate: Results from a Meadow-Warming Experiment.
766   Ecological Applications 5, 132–150. doi:10.2307/1942058
767   Hashimoto, S., Komatsu, H., 2006. Relationships between soil CO_2 concentration and CO_2
768   production, temperature, water content, and gas diffusivity: implications for field studies
769   through sensitivity analyses. Journal of Forest Research 11, 41–50. doi:10.1007/s10310-
770   005-0185-4
771   Herbst, M., Tappe, W., Kummer, S., Vereecken, H., 2016. The impact of sieving on
772   heterotrophic respiration response to water content in loamy and sandy topsoils.
773   Geoderma 272, 73–82. doi:10.1016/j.geoderma.2016.03.002
774   Howard, D.M., Howard, P.J.A., 1993. Relationships between co2 evolution, moisture content
775   and temperature for a range of soil types. Soil Biology and Biochemistry 25, 1537–1546.
776   doi:10.1016/0038-0717(93)90008-Y
777   Husen, E., Salma, S., Agus, F., 2014. Peat emission control by groundwater management and
778   soil amendments: evidence from laboratory experiments. Mitigation and Adaptation
779   Strategies for Global Change 19, 821–829. doi:10.1007/s11027-013-9526-3
780   Inglima, I., ALBERTI, G., BERTOLINI, T., VACCARI, F.P., GIOLI, B., MIGLIETTA, F.,
781   COTRUFO, M.F., PERESSOTTI, A., 2009. Precipitation pulses enhance respiration of
782   Mediterranean ecosystems: the balance between organic and inorganic components of
783   increased soil CO_2 efflux. Global Change Biology 15, 1289–1301. doi:10.1111/j.1365-
784   2486.2008.01793.x
785   Iovieno, P., Bååth, E., 2008. Effect of drying and rewetting on bacterial growth rates in soil.
786   FEMS Microbiology Ecology 65, 400. doi:10.1111/j.1574-6941.2008.00524.x
787   Jia, B., Zhou, G., Yuan, W., 2007. Modeling and coupling of soil respiration and soil water
788   content in fenced Leymus chinensis steppe, Inner Mongolia. Ecological Modelling 201,
789   157–162. doi:10.1016/j.ecolmodel.2006.09.008
790   Jin, X., Wang, S., Zhou, Y., 2008. Microbial CO_2 production from surface and subsurface soil as
791   affected by temperature, moisture, and nitrogen fertilisation. Soil Research 46, 273–280.
792   Kang, S., Doh, S., Lee, D., Lee, D., Jin, V.L., Kimball, J.S., 2003. Topographic and climatic
793   controls on soil respiration in six temperate mixed-hardwood forest slopes, Korea. Global
794   Change Biology 9, 1427–1437. doi:10.1046/j.1365-2486.2003.00668.x
795   Kant, R., Ghosh, C., Singh, L., Tripathi, N., 2011. Effect of Bacterial and Fungal Abundance in
796   Soil on the Emission of Carbon Dioxide from Soil in Semi-arid Climate in India, in:
797   Gökçekus, H., Türker, U., LaMoreaux, J.W. (Eds.), Survival and Sustainability:
798   Environmental Concerns in the 21st Century. Springer Berlin Heidelberg, Berlin,
799   Heidelberg, pp. 151–161.
800   Kieft, T.L., soroker, E., firestone, M.K., 1987. Microbial biomass response to a rapid increase in
801   water potential when dry soil is wetted. Soil Biology and Biochemistry 19, 119–126.
802   doi:10.1016/0038-0717(87)90070-8
803   Kim, D.-G., Mu, S., Kang, S., Lee, D., 2010. Factors controlling soil CO_2 effluxes and the
804   effects of rewetting on effluxes in adjacent deciduous, coniferous, and mixed forests in
805   Korea. Soil Biology and Biochemistry 42, 576–585. doi:10.1016/j.soilbio.2009.12.005
806   Kirschbaum, M.U.F., 1995. The temperature dependence of soil organic matter decomposition,
807   and the effect of global warming on soil organic C storage. Soil Biology and
808   Biochemistry 27, 753–760. doi:10.1016/0038-0717(94)00242-S

809 Lauber, C.L., Ramirez, K.S., Aanderud, Z., Lennon, J., Fierer, N., 2013. Temporal variability in
810   soil microbial communities across land-use types. ISME J 7, 1641–1650.
811 Lawrence, C.R., Neff, J.C., Schimel, J.P., 2009. Does adding microbial mechanisms of
812   decomposition improve soil organic matter models? A comparison of four models using
813   data from a pulsed rewetting experiment. Soil Biology and Biochemistry 41, 1923–1934.
814   doi:10.1016/j.soilbio.2009.06.016
815 Lellei-Kovács, E., Botta-Dukát, Z., de Dato, G., Estiarte, M., Guidolotti, G., Kopittke, G.R.,
816   Kovács-Láng, E., Kröel-Dulay, G., Larsen, K.S., Peñuelas, J., Smith, A.R., Sowerby, A.,
817   Tietema, A., Schmidt, I.K., 2016. Temperature Dependence of Soil Respiration
818   Modulated by Thresholds in Soil Water Availability Across European Shrubland
819   Ecosystems. Ecosystems 19, 1460–1477. doi:10.1007/s10021-016-0016-9
820 Lennon, J.T., Jones, S.E., 2011. Microbial seed banks: the ecological and evolutionary
821   implications of dormancy. Nat Rev Micro 9, 119–130. doi:10.1038/nrmicro2504
822 Li, X., Ishikura, K., Wang, C., Yeluripati, J., Hatano, R., 2015. Hierarchical Bayesian models for
823   soil CO2 flux using soil texture: a case study in central Hokkaido, Japan. Soil Science
824   and Plant Nutrition 61, 116–132. doi:10.1080/00380768.2014.978728
825 Li, Y., Xu, M., Zou, X., 2006. Heterotrophic Soil Respiration in Relation to Environmental
826   Factors and Microbial Biomass in Two Wet Tropical Forests. Plant and Soil 281, 193–
827   201. doi:10.1007/s11104-005-4249-1
828 Lloyd, J., Taylor, J.A., 1994. On the Temperature Dependence of Soil Respiration. Functional
829   Ecology 8, 315–323. doi:10.2307/2389824
830 Loeppert, R.H., Suarez, D.L., 1996. Carbonate and Gympsum, in: Methods of Soil Analysis. Part
831   3. Chemical Methods--SSSA, 5. Soil Science Society of America and American Society
832   of Agronomy, Madison, WI, USA, pp. 455–456.
833 Long, P.E., Williams, K.H., Davis, J.A., Fox, P.M., Wilkins, M.J., Yabusaki, S.B., Fang, Y.,
834   Waichler, S.R., Berman, E.S.F., Gupta, M., Chandler, D.P., Murray, C., Peacock, A.D.,
835   Giloteaux, L., Handley, K.M., Lovley, D.R., Banfield, J.F., 2015. Bicarbonate impact on
836   U(VI) bioreduction in a shallow alluvial aquifer. Geochimica et Cosmochimica Acta 150,
837   106–124. doi:10.1016/j.gca.2014.11.013
838 Luo, Y., Ahlström, A., Allison, S.D., Batjes, N.H., Brovkin, V., Carvalhais, N., Chappell, A.,
839   Ciais, P., Davidson, E.A., Finzi, A., Georgiou, K., Guenet, B., Hararuk, O., Harden, J.W.,
840   He, Y., Hopkins, F., Jiang, L., Koven, C., Jackson, R.B., Jones, C.D., Lara, M.J., Liang,
841   J., McGuire, A.D., Parton, W., Peng, C., Randerson, J.T., Salazar, A., Sierra, C.A., Smith,
842   M.J., Tian, H., Todd-Brown, K.E.O., Torn, M., van Groenigen, K.J., Wang, Y.P., West,
843   T.O., Wei, Y., Wieder, W.R., Xia, J., Xu, X., Xu, X., Zhou, T., 2016. Toward more
844   realistic projections of soil carbon dynamics by Earth system models. Global
845   Biogeochemical Cycles 30, 40–56. doi:10.1002/2015GB005239
846 Manzoni, S., Moyano, F., Kätterer, T., Schimel, J., 2016. Modeling coupled enzymatic and
847   solute transport controls on decomposition in drying soils. Soil Biology and Biochemistry
848   95, 275–287. doi:10.1016/j.soilbio.2016.01.006
849 Manzoni, S., Schaeffer, S.M., Katul, G., Porporato, A., Schimel, J.P., 2014. A theoretical
850   analysis of microbial eco-physiological and diffusion limitations to carbon cycling in
851   drying soils. Soil Biology and Biochemistry 73, 69–83. doi:10.1016/j.soilbio.2014.02.008
852 Manzoni, S., Schimel, J.P., Porporato, A., 2012. Responses of soil microbial communities to
853   water stress: results from a meta-analysis. Ecology 93, 930–938. doi:10.1890/11-0026.1

854 Markstrom, S.L., Hay, L.E., 2009. Integrated Watershed Scale Response to Climate Change for
855   Selected Basins Across the United States. Water Resources IMPACT 11, 8–10.
856 Martiny, A.C., Treseder, K., Pusch, G., 2013. Phylogenetic conservatism of functional traits in
857   microorganisms. ISME J 7, 830–838.
858 Meisner, A., Rousk, J., Bååth, E., 2015. Prolonged drought changes the bacterial growth
859   response to rewetting. Soil Biology and Biochemistry 88, 314–322.
860   doi:10.1016/j.soilbio.2015.06.002
861 Mielnick, P.C., Dugas, W.A., 2000. Soil CO_2 flux in a tallgrass prairie. Soil Biology and
862   Biochemistry 32, 221–228. doi:10.1016/S0038-0717(99)00150-9
863 Miller, A.E., Schimel, J.P., Meixner, T., Sickman, J.O., Melack, J.M., 2005. Episodic rewetting
864   enhances carbon and nitrogen release from chaparral soils. Soil Biology and
865   Biochemistry 37, 2195–2204. doi:10.1016/j.soilbio.2005.03.021
866 Moncrieff, J.B., Fang, C., 1999. A model for soil CO_2 production and transport 2: Application to
867   a florida Pinus elliotte plantation. Agricultural and Forest Meteorology 95, 237–256.
868   doi:10.1016/S0168-1923(99)00035-0
869 Monson, R.K., Lipson, D.L., Burns, S.P., Turnipseed, A.A., Delany, A.C., Williams, M.W.,
870   Schmidt, S.K., 2006. Winter forest soil respiration controlled by climate and microbial
871   community composition. Nature 439, 711–714. doi:10.1038/nature04555
872 Moyano, F.E., Manzoni, S., Chenu, C., 2013. Responses of soil heterotrophic respiration to
873   moisture availability: An exploration of processes and models. Soil Biology and
874   Biochemistry 59, 72–85. doi:10.1016/j.soilbio.2013.01.002
875 Moyano, F.E., Vasilyeva, N., Bouckaert, L., Cook, F., Craine, J., Curiel Yuste, J., Don, A.,
876   Epron, D., Formanek, P., Franzluebbers, A., Ilstedt, U., Kätterer, T., Orchard, V.,
877   Reichstein, M., Rey, A., Ruamps, L., Subke, J.-A., Thomsen, I.K., Chenu, C., 2012. The
878   moisture response of soil heterotrophic respiration: Interaction with soil properties.
879   Biogeosciences 9, 1173–1182. doi:10.5194/bg-9-1173-2012
880 Niklińska, M., Klimek, B., 2007. Effect of temperature on the respiration rate of forest soil
881   organic layer along an elevation gradient in the Polish Carpathians. Biology and Fertility
882   of Soils 43, 511–518. doi:10.1007/s00374-006-0129-y
883 Orchard, V.A., Cook, F.J., 1983. Relationship between soil respiration and soil moisture. Soil
884   Biology and Biochemistry 15, 447–453. doi:10.1016/0038-0717(83)90010-X
885 Parton, W.J., Schimel, D.S., Cole, C.V., Ojima, D.S., 1987. Analysis of Factors Controlling Soil
886   Organic Matter Levels in Great Plains Grasslands1. Soil Science Society of America
887   Journal 51, 1173–1179. doi:10.2136/sssaj1987.03615995005100050015x
888 Paul, K.I., Polglase, P.J., O'Connell, A.M., Carlyle, J.C., Smethurst, P.J., Khanna, P.K., 2003.
889   Defining the relation between soil water content and net nitrogen mineralization.
890   European Journal of Soil Science 54, 39–48. doi:10.1046/j.1365-2389.2003.00502.x
891 Persson, H., Von Fircks, Y., Majdi, H., Nilsson, L.O., 1995. Root distribution in a Norway
892   spruce (Picea abies (L.) Karst.) stand subjected to drought and ammonium-sulphate
893   application. Plant and Soil 168, 161–165. doi:10.1007/BF00029324
894 PINGINTHA, N., LECLERC, M.Y., BEASLEY Jr., J.P., ZHANG, G., SENTHONG, C., 2010.
895   Assessment of the soil CO_2 gradient method for soil CO_2 efflux measurements:
896   comparison of six models in the calculation of the relative gas diffusion coefficient.
897   Tellus B 62, 47–58. doi:10.1111/j.1600-0889.2009.00445.x

898   Placella, S.A., Brodie, E.L., Firestone, M.K., 2012. Rainfall-induced carbon dioxide pulses result
899   from sequential resuscitation of phylogenetically clustered microbial groups. Proceedings
900   of the National Academy of Sciences 109, 10931–10936. doi:10.1073/pnas.1204306109
901   Porporato, A., D'Odorico, P., Laio, F., Rodriguez-Iturbe, I., 2003. Hydrologic controls on soil
902   carbon and nitrogen cycles. I. Modeling scheme. Advances in Water Resources 26, 45–58.
903   doi:10.1016/S0309-1708(02)00094-5
904   Pumpanen, J., Ilvesniemi, H., Hari, P., 2003. A Process-Based Model for Predicting Soil Carbon
905   Dioxide Efflux and Concentration. Soil Science Society of America Journal 67, 402–413.
906   doi:10.2136/sssaj2003.4020
907   Reichstein, M., Rey, A., Freibauer, A., Tenhunen, J., Valentini, R., Banza, J., Casals, P., Cheng,
908   Y., Grünzweig, J.M., Irvine, J., Joffre, R., Law, B.E., Loustau, D., Miglietta, F., Oechel,
909   W., Ourcival, J.-M., Pereira, J.S., Peressotti, A., Ponti, F., Qi, Y., Rambal, S., Rayment,
910   M., Romanya, J., Rossi, F., Tedeschi, V., Tirone, G., Xu, M., Yakir, D., 2003. Modeling
911   temporal and large-scale spatial variability of soil respiration from soil water availability,
912   temperature and vegetation productivity indices. Global Biogeochemical Cycles 17, n/a-
913   n/a. doi:10.1029/2003GB002035
914   Rey, A., Petsikos, C., Jarvis, P.G., Grace, J., 2005. Effect of temperature and moisture on rates of
915   carbon mineralization in a Mediterranean oak forest soil under controlled and field
916   conditions. European Journal of Soil Science 56, 589–599. doi:10.1111/j.1365-
917   2389.2004.00699.x
918   Sanaullah, M., Rumpel, C., Charrier, X., Chabbi, A., 2012. How does drought stress influence
919   the decomposition of plant litter with contrasting quality in a grassland ecosystem? Plant
920   and Soil 352, 277–288. doi:10.1007/s11104-011-0995-4
921   Schimel, J.P., Schaeffer, S.M., 2015. Microbial control over carbon cycling in soil. The Causes
922   and Consequences of Microbial Community Structure 22, 155.
923   Schimel, J.P., Weintraub, M.N., 2003. The implications of exoenzyme activity on microbial
924   carbon and nitrogen limitation in soil: a theoretical model. Soil Biology and Biochemistry
925   35, 549–563. doi:10.1016/S0038-0717(03)00015-4
926   Schjønning, P., Thomsen, I.K., Moldrup, P., Christensen, B.T., 2003. Linking Soil Microbial
927   Activity to Water- and Air-Phase Contents and Diffusivities. Soil Science Society of
928   America Journal 67, 156–165. doi:10.2136/sssaj2003.1560
929   Shi, A., Marschner, P., 2014. Drying and rewetting frequency influences cumulative respiration
930   and its distribution over time in two soils with contrasting management. Soil Biology and
931   Biochemistry 72, 172–179. doi:10.1016/j.soilbio.2014.02.001
932   Skopp, J., Jawson, M.D., Doran, J.W., 1990. Steady-State Aerobic Microbial Activity as a
933   Function of Soil Water Content. Soil Science Society of America Journal 54, 1619–1625.
934   doi:10.2136/sssaj1990.03615995005400060018x
935   Stevenson, L.H., 1977. A case for bacterial dormancy in aquatic systems. Microbial Ecology 4,
936   127–133. doi:10.1007/BF02014283
937   Tian, D., Wang, G., Yan, W., Xiang, W., Peng, C., 2010. Soil respiration dynamics in
938   Cinnamomum camphora forest and a nearby Liquidambar formosana forest in
939   Subtropical China. Chinese Science Bulletin 55, 736–743. doi:10.1007/s11434-009-
940   0452-4
941   Todd-Brown, K.E.O., Randerson, J.T., Post, W.M., Hoffman, F.M., Tarnocai, C., Schuur, E.A.G.,
942   Allison, S.D., 2013. Causes of variation in soil carbon simulations from CMIP5 Earth
943   system models and comparison with observations. doi:10.5194/bg-10-1717-2013

944 Unger, S., Máguas, C., Pereira, J.S., David, T.S., Werner, C., 2010. The influence of
945   precipitation pulses on soil respiration – Assessing the "Birch effect" by stable carbon
946   isotopes. Soil Biology and Biochemistry 42, 1800–1810.
947   doi:10.1016/j.soilbio.2010.06.019
948 Vanhala, P., 2002. Seasonal variation in the soil respiration rate in coniferous forest soils. Soil
949   Biology and Biochemistry 34, 1375–1379. doi:10.1016/S0038-0717(02)00061-5
950 Vanhala, P., Karhu, K., Tuomi, M., Björklöf, K., Fritze, H., Liski, J., 2008. Temperature
951   sensitivity of soil organic matter decomposition in southern and northern areas of the
952   boreal forest zone. Soil Biology and Biochemistry 40, 1758–1764.
953   doi:10.1016/j.soilbio.2008.02.021
954 VANHALA, P., TAMMINEN, P., FRITZE, H., 2005. RELATIONSHIP BETWEEN BASAL
955   SOIL RESPIRATION RATE, TREE STAND AND SOIL CHARACTERISTICS IN
956   BOREAL FORESTS. Environmental Monitoring and Assessment 101, 85–92.
957   doi:10.1007/s10661-005-9134-0
958 Verburg, P.S.J., Larsen, J., Johnson, D.W., Schorran, D.E., Arnone, J.A., 2005. Impacts of an
959   anomalously warm year on soil CO2 efflux in experimentally manipulated tallgrass
960   prairie ecosystems. Global Change Biology 11, 1720–1732. doi:10.1111/j.1365-
961   2486.2005.001032.x
962 Wagle, P., Kakani, V.G., 2014. Confounding Effects of Soil Moisture on the Relationship
963   Between Ecosystem Respiration and Soil Temperature in Switchgrass. BioEnergy
964   Research 7, 789–798. doi:10.1007/s12155-014-9434-8
965 Wang, G., Jagadamma, S., Mayes, M.A., Schadt, C.W., Megan Steinweg, J., Gu, L., Post, W.M.,
966   2015. Microbial dormancy improves development and experimental validation of
967   ecosystem model. ISME J 9, 226–237.
968 Wang, X., Li, X., Hu, Y., Lv, J., Sun, J., Li, Z., Wu, Z., 2010. Effect of temperature and moisture
969   on soil organic carbon mineralization of predominantly permafrost peatland in the Great
970   Hing'an Mountains, Northeastern China. Journal of Environmental Sciences 22, 1057–
971   1066. doi:10.1016/S1001-0742(09)60217-5
972 Welsch, D.L., Hornberger, G.M., 2004. Spatial and temporal simulation of soil CO2
973   concentrations in a small forested catchment in Virginia. Biogeochemistry 71, 413–434.
974   doi:10.1023/B:BIOG.0000049350.24911.e9
975 Winnick, M.J., Carroll, R.W.H., Williams, K.H., Maxwell, R.M., Dong, W., Maher, K., 2017.
976   Snowmelt controls on concentration-discharge relationships and the balance of oxidative
977   and acid-base weathering fluxes in an alpine catchment, East River, Colorado. Water
978   Resources Research 53, 2507–2523. doi:10.1002/2016WR019724
979 Wu, H.-J., Lee, X., 2011. Short-term effects of rain on soil respiration in two New England
980   forests. Plant and Soil 338, 329–342. doi:10.1007/s11104-010-0548-2
981 Xu, L., Baldocchi, D.D., Tang, J., 2004. How soil moisture, rain pulses, and growth alter the
982   response of ecosystem respiration to temperature. Global Biogeochemical Cycles 18, n/a-
983   n/a. doi:10.1029/2004GB002281
984 Yan, L., Chen, S., Xia, J., Luo, Y., 2014. Precipitation Regime Shift Enhanced the Rain Pulse
985   Effect on Soil Respiration in a Semi-Arid Steppe. PLoS ONE 9, e104217.
986   doi:10.1371/journal.pone.0104217
987

Biogeosciences
Open Access
Discussions
EGU

Table 1. Soil carbon content over a range of aggregated depths measured by EA.

Sample Name	Depth	Carbon (wt. %)	Carbon stdev	Total Organic Carbon (wt. %)	Total Organic Carbon stdev	Total Inorganic carbon (wt. %)
BCM.top.1	0-52	2.64	0.03	2	0.41	0.63
BCM.top.2	0-52	2.54	0.05	2.07	0.32	0.46
BCM.mid.1	63-108	1.71	0.01	1.44	0.08	0.27
BCM.mid.2	63-108	1.67	0.06	1.43	0.02	0.23
BCM.bot.1	112-165	1.04	0.12	0.9	0.02	0.14
BCM.bot.2	112-165	0.96	0.01	0.89	0.03	0.07

988
989

Biogeosciences
Open Access
Discussions
EGU

Table 2. CO_2 respiration data from incubation experiments.

			Incubation time (h)						
			0	24	48.5	72.5	96	139.5	186.5
	Soil depth (cm)	Moisture content (%)	CO_2 flux (μmol/g soil/day)						
BCM-top-0	0-52	0	0	0.151	0.080	0.064	0.038	0.026	0.028
BCM-top-1		33	0	3.106	2.189	1.689	1.449	1.150	0.902
BCM-top-2		66	0	4.808	5.307	3.222	2.310	1.697	1.317
BCM-top-3		100	0	2.585	2.906	2.662	2.118	1.711	1.563
BCM-mid-0	63-108	0	0	0.309	0.216	0.163	0.101	0.077	0.071
BCM-mid-1		33	0	1.705	1.392	1.116	0.795	0.646	0.562
BCM-mid-2		66	0	2.235	3.188	2.084	1.257	0.909	0.795
BCM-mid-3		100	0	1.181	1.669	1.320	1.034	0.870	0.831
BCM-bot-0	112-165	0	0	0.406	0.253	0.178	0.096	0.063	0.061
BCM-bot-1		33	0	1.279	0.667	0.469	0.258	0.183	0.177
BCM-bot-2		66	0	1.140	0.834	0.664	0.385	0.309	0.296
BCM-bot-3		100	0	0.610	0.553	0.366	0.365	0.318	0.299

990

991

Biogeosciences Open Access
Discussions
EGU

Table 3. Parameter inputs for the first-order model.

	FO1	FO2	Description
PARAMETER			
$k_{sol,1}$ (1/hour)	N/A	5.00E-04	
$k_{sol,2}$ (1/hour)	5.00E-05	5.00E-05	Decomposition rate constant
f_s (unitless)	0.1	0.1	Porportion of carbon used for microbial growth
f_e (unitless)	0.9	0.9	Porportion of carbon used for microbial respiration
$k_{up,1}$ (1/hour)	N/A	4.00E-02	Microbial uptake rate constant for fast-responding biomass
$k_{up,2}$ (1/hour)	2.00E-02	2.00E-02	Microbial uptake rate constant for slow-responding biomass
k_{mor}	4.17E-05	4.17E-05	Mortality rate constant for biomass
$Se_{thres,1}$ (unitless)	N/A	0.25	Threshold effective saturation
$Se_{thres,2}$ (unitless)	0.6	0.55	Threshold effective saturation
INIT. CONDITION			
Se	Variable	Variable	
C (mass fraction)	0.02	0.02 (upper), 0.014 (middle), 0.009 (lower)	Total carbon fraction
C_{total} (gC/m³H₂O)	C*1518720	C*1518720	Total carbon concentration (unit converted from C)
$C_{sub,1}$ (gC/m³H₂O)	N/A	$1/4*0.875*C_{total}$	Concentration for substration carbon
$C_{sub,2}$ (gC/m³H₂O)	$0.88*C_{total}$	$3/4*0.88*C_{total}$	Concentration for substration carbon
$C_{soluble,1}$ (gC/m³H₂O)	N/A	$1/4*0.025*C_{total} \pm 20\%$	Concentration for soluble carbon
$C_{soluble,2}$ (gC/m³H₂O)	$0.02*C_{total} \pm 20\%$	$3/4*0.02*C_{total} \pm 20\%$	Concentration for soluble carbon
Bio_1 (gC/m³H₂O)	N/A	$1/4*0.1*C_{total}$	Concentration for fast-responding biomass
Bio_2 (gC/m³H₂O)	$0.1*C_{total}$	$3/4*0.1*C_{total}$	Concentration for slow-responding biomass

992

993

Table 4. Parameter inputs for the dormancy models.

	DM1	DM2	Description
PARAMETER			
a (unitless)	20	20	Transition coefficient
$k_{sol,1}$ (1/hour)	N/A	9.38E-05	Decomposition rate constant
$k_{sol,2}$ (1/hour)	4.17E-05	1.39E-05	Decomposition rate constant
f_s (unitless)	0.1	0.1	Porportion of carbon used for microbial growth
f_r (unitless)	0.9	0.9	Porportion of carbon used for microbial respiration
$k_{up,1}$ (1/hour)	N/A	1	Microbial uptake rate constant for fast-responding biomass
$k_{up,2}$ (1/hour)	8	4	Microbial uptake rate constant for slow-responding biomass
$C_{half,1}$ (gC/m^3)	N/A	15000	Half saturation for soluble carbon
$C_{half,2}$ (gC/m^3)	45000	45000	Half saturation for soluble carbon
K_{half}	N/A	N/A	Half saturation for O_2
$k_{tran,1}$ (1/hour)	N/A	1	Transition rate constant between active and dormant biomass for fast-responding biomass
$k_{tran,2}$ (1/hour)	0.017	0.017	Transition rate constant between active and dormant biomass for slow-responding biomass
$Se_{half,1}$ (unitless)	N/A	0.25	Half saturation for effective saturation for fast-responding biomass
$Se_{half,2}$ (unitless)	0.55	0.55	Half saturation for effective saturation for slow-responding biomass
b (unitless)	4.9	4.9	Pore size distribution parameter
k_{mor-a}	4.17E-05	4.17E-05	Mortality rate constant for active biomass
k_{mor-d}	4.17E-06	4.17E-06	Mortality rate constant for dormant biomass
INIT. CONDITION			
Se	Variable	Variable	
C (mass fraction)	0.02	0.02 (upper), 0.014 (middle), 0.009 (lower)	Total carbon fraction
C_{total} (gC/m^3H_2O)	C*1518720/Se	C*1518720/Se	Total carbon concentration (unit converted from C)
$C_{sub,1}$ (gC/m^3H_2O)	N/A	1/4*0.875*C_{total}	Concentration for substration carbon
$C_{sub,2}$ (gC/m^3H_2O)	0.893*C_{total}	3/4*0.894*C_{total}	Concentration for substration carbon
$C_{soluble,1}$ (gC/m^3H_2O)	N/A	1/4*0.025*C_{total} ± 20%	Concentration for soluble carbon
$C_{soluble,2}$ (gC/m^3H_2O)	0.007*C_{total} ± 20%	3/4*0.006*C_{total} ± 20%	Concentration for soluble carbon
$Bio_{active,1}$ (gC/m^3H_2O)	N/A	0	Concentration for fast-responding active biomass
$Bio_{active,2}$ (gC/m^3H_2O)	0	0	Concentration for slow-responding active biomass
$Bio_{dormant,1}$ (gC/m^3H_2O -undiluted)	N/A	1/4*0.1*C_{total} *Se	Concentration for fast-responding dormant biomass
$Bio_{dormant,2}$ (gC/m^3H_2O -undiluted)	0.1*C_{total} *Se	3/4*0.1*C_{total} *Se	Concentration for slow-responding dormant biomass

994

995

Table 5. AIC values of the two models.

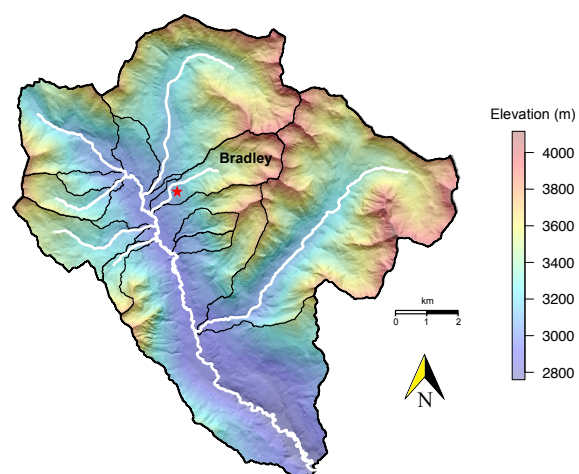|	FO1	DM2
Shallow-66%Se	33.0269	21.8236
Shallow-33%Se	25.9891	10.4347
Intermediate-66%Se	28.1768	26.9186
Intermediate-33%Se	21.6725	9.0794
Deep-66%Se	22.8723	34.3137
Deep-33%Se	16.541	22.764

996

997

Fig 1. The East River watershed within the Gunnison River basin, Colorado, USA (the drainage paths are shown in white line). The red star illustrates the location where the soil incubation samples were collected for the current study (38°59'8.42" N, 107°0'12.51" W).

998
999
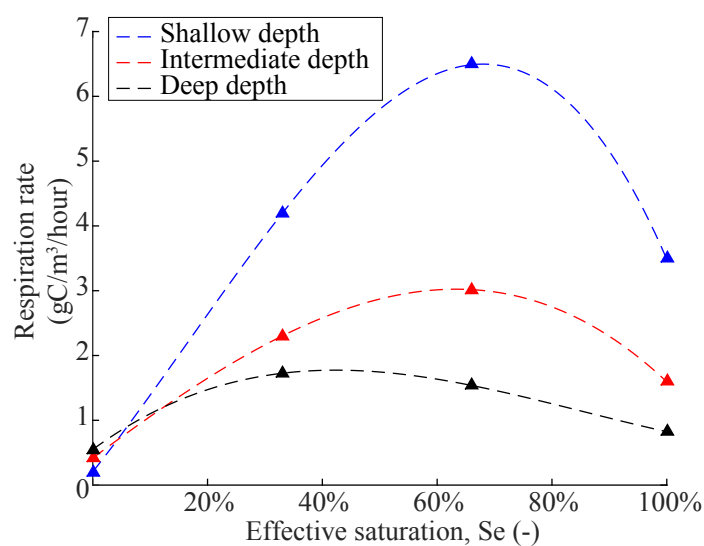
Fig 2. Respiration rate as a function of four values of *Se* (filled triangles) fitted with dashed lines to illustrate trends. Measurement uncertainties lie within symbols (<1.5 % of the measured concentration). Soil respiration rates are shown for the first 24 hours of incubation for all three soil depths (0-52 cm (blue), 63-108 cm (red) and 112-165 cm (black)) at different effective saturations (Se = 0, 33 %, 66 % and 100 %).

1000
1001
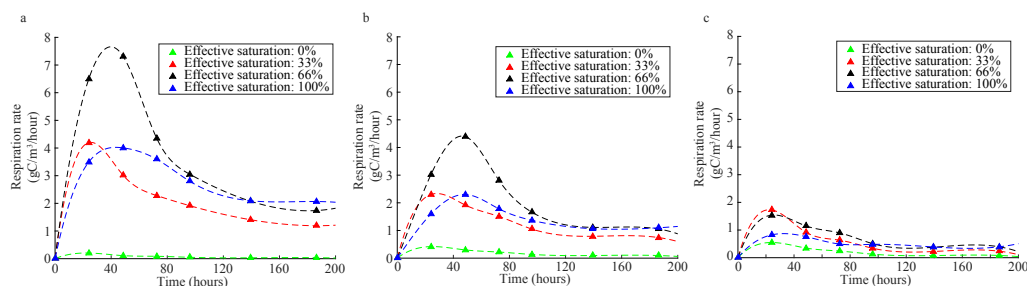
Fig 3. Respiration rate for (a) shallow soil sample (0-52 cm); (b) intermediate soil samples (63-108 cm); (c) deep soil samples (112-165 cm), as a function of time for four values of *Se* (filled triangles) fitted with dashed lines (cubic interpolation) to illustrate trends. Measurement uncertainties lie within symbols (<1.5 % of the measured concentration).

1002

1003
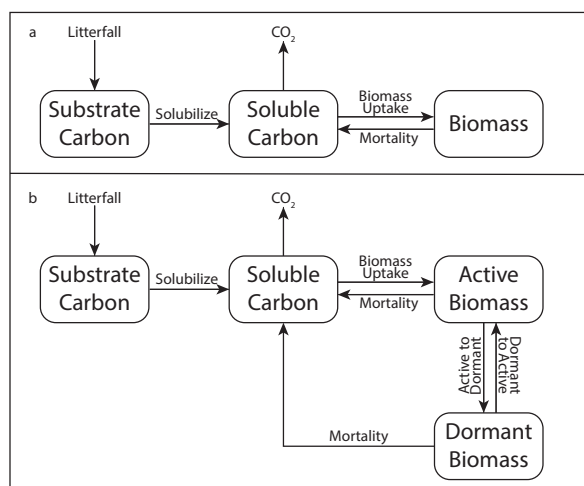
Fig 4. The conceptual models for both: (a) First-order, and (b) dormancy (adjusted from Manzoni et al. (2014)). Boxes indicate distinct carbon pools, and arrows indicate the reactive pathways of carbon between the pools.

1004
1005
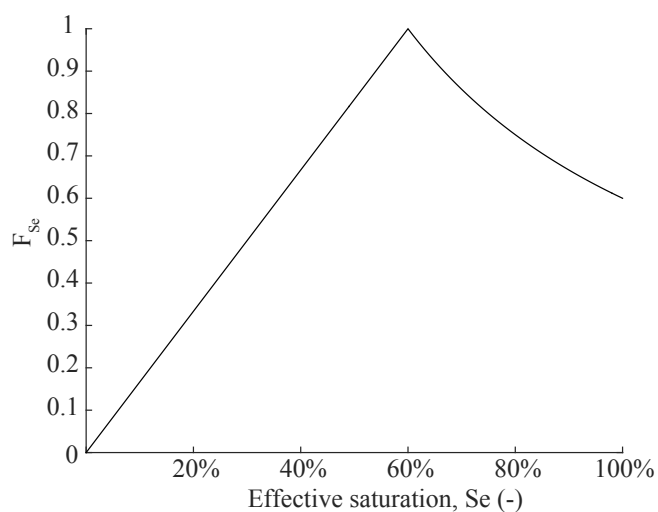
Fig 5. The non-dimensional factor F_{Se} as a function of effective satura-
tion. F_{Se} reaches 1 where Se_{thres} is set (60 % in this study).

1006
1007
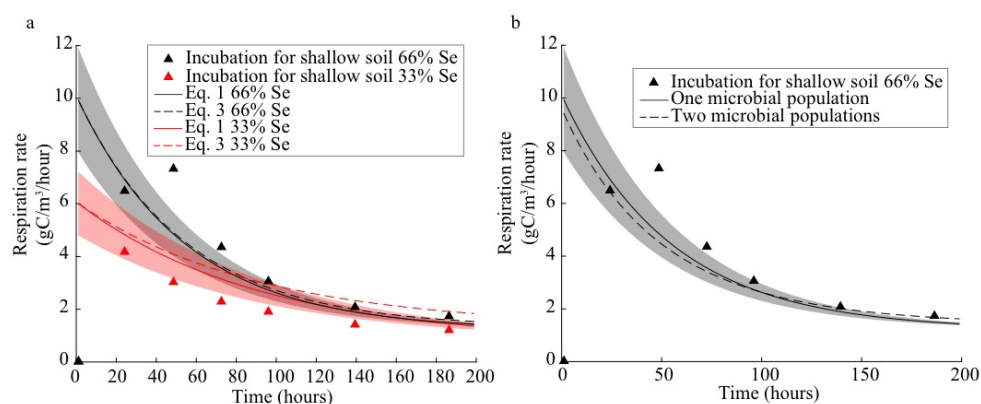
Fig 6. The first-order kinetic model using (a) FO1; Solid lines represent model uses moisture dependent solubilization law (Eq. (1)), and dashed lines represent model uses moisture independent solubilization law (Eq. (3)); (b) FO1 (solid line) and FO2 (dashed line) microbial populations (all parameters shown in Table 3). Shaded areas represent range of model output with the initial soluble carbon concentration varied by 20 %. This variation is further discussed in Sect. 5.1.

1008

1009
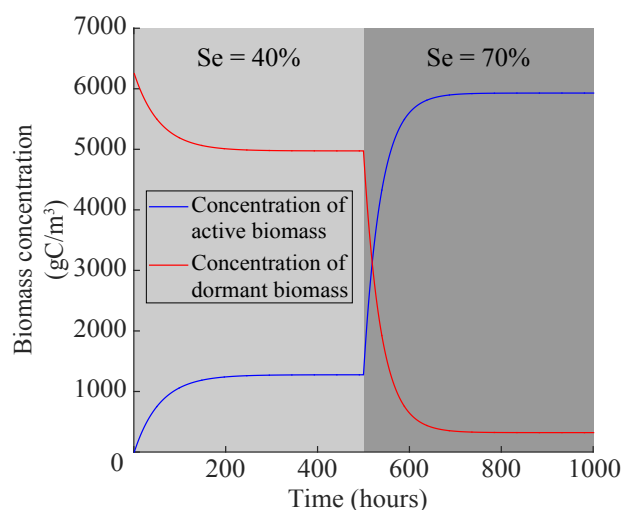
Fig 7. Transition between active and dormant biomass as a function of Eq. (8) and (9). Starting active and dormant biomass concentrations are set to 0 and 6250 gC m^{-3}, respectively. As the simulation begins, an initial Se_{sample} of 40 % has been present for a sufficient period of time such that the active and dormant biomass pools are in steady state. At a time t = 500 hours, the Se_{sample} is increased to a new value of 70 %, leading to a shift in the distribution of active and dormant biomass.

1010
1011

Biogeosciences
Discussions
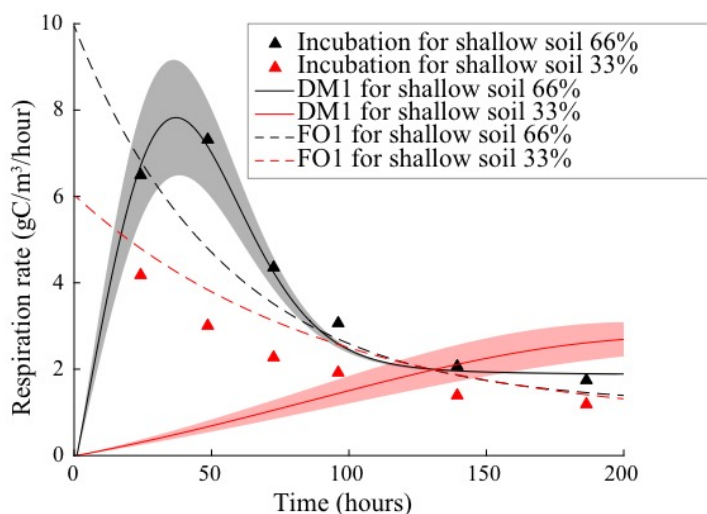
Fig 8. Comparison of model and measured respiration rates for the shallow soil 33 % and 66 % *Se* values as a function of time. Filled triangles represent experimental data, and lines illustrate output from DM1. Shaded areas represent range of model output with the initial soluble carbon concentration varied by 20 %. FO1 outputs (dashed lines) are also plotted here for comparison. This variation is further discussed in Sect. 5.1.
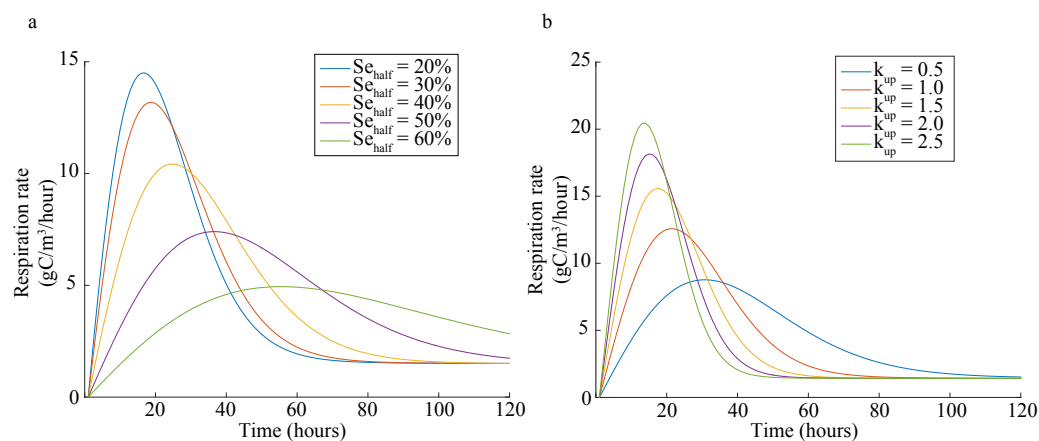
1012
1013

Fig 9. (a) Model sensitivity to a range of Se_{half} values, with all other parameters held constant (Table 4). Different colors represent different Se_{half}. (b) Model sensitivity to a range of k_{up} values, with other conditions similar to (a).

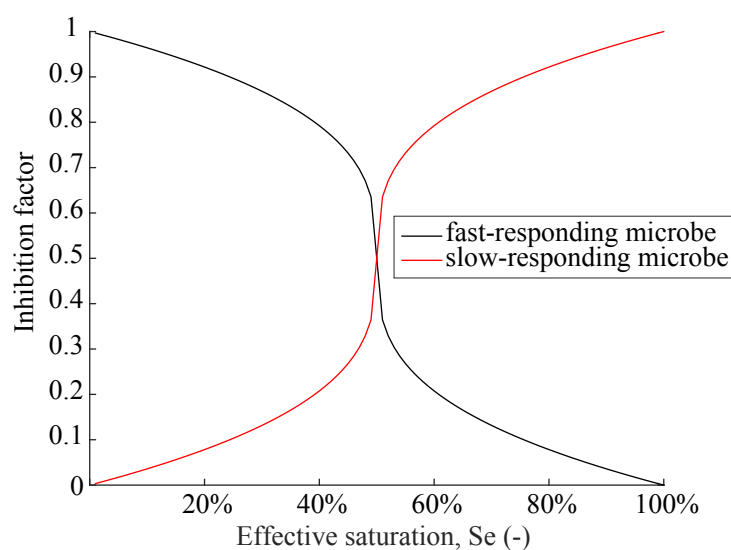1014

1015

Biogeosciences
Discussions

Open Access

EGU

Fig 10. Inhibition factor for both fast- and slow-responding
microbial populations as a function of *Se* (Eq. (10) & (11)).
The red line represents the slow-responding population,
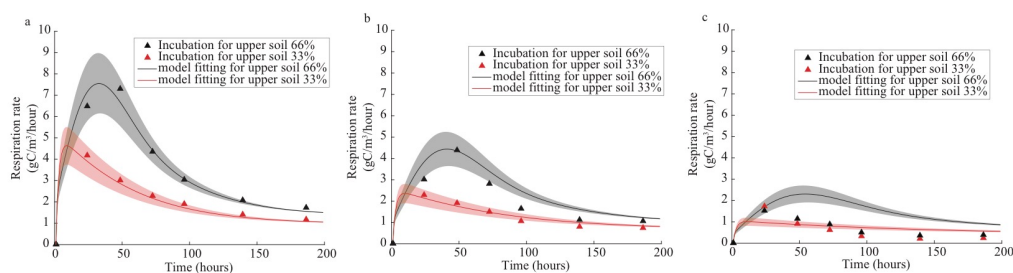while the black line represents fast-responders.

1016
1017

Fig 11. The performance of DM2 when simulating (a) upper soil; (b) middle soil; (c) lower soil at both 33 % and 66 % Se. Shaded areas represent range of model output with the initial soluble carbon concentration varied by 20 %. This variation is further discussed in Sect 5.1.
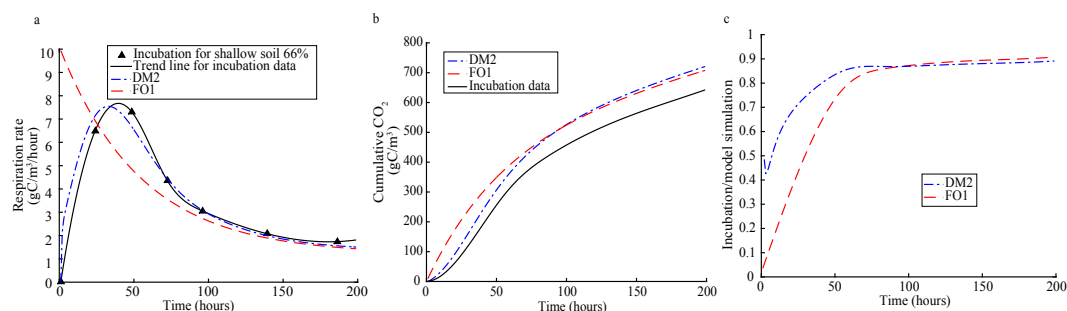
1018

1019

Fig 12. (a) Model output from FO1 and DM2 plotted against incubation data in time series. Measurement uncertainties lie within symbols (<1.5 % of the measured concentration). Parameter values for two models are listed in Table 3 and 4; (b) Cumulative CO_2 concentration integrated from model output and trend line shown in (a); (c) Ratio of integrated incubation data/model output shown in (b) for two models. The dormancy model is clearly a better simulation compared to first-order model within 100 hours (closer to 1).

1020